

PAPER • OPEN ACCESS

Fitness effects of a demography-dispersal trade-off in expanding *Saccharomyces cerevisiae* mats

To cite this article: Rebekah Hall *et al* 2024 *Phys. Biol.* **21** 026001

View the [article online](#) for updates and enhancements.

You may also like

- [Large scale climate oscillation impacts on temperature, precipitation and land surface phenology in Central Asia](#)
Kirsten M de Beurs, Geoffrey M Henebry, Braden C Owsley et al.
- [Transpiration cooling with bio-inspired structured surfaces](#)
Gan Huang, Yinhai Zhu, Zhi-Yuan Liao et al.
- [Black hole demography: from scaling relations to models](#)
Francesco Shankar

Physical Biology



PAPER

OPEN ACCESS

RECEIVED
12 April 2023

REVISED
21 December 2023

ACCEPTED FOR PUBLICATION
9 January 2024

PUBLISHED
22 January 2024

Original Content from
this work may be used
under the terms of the
[Creative Commons
Attribution 4.0 licence](#).

Any further distribution
of this work must
maintain attribution to
the author(s) and the title
of the work, journal
citation and DOI.



Fitness effects of a demography-dispersal trade-off in expanding *Saccharomyces cerevisiae* mats

Rebekah Hall^{1,4,5} , Akila Bandara^{2,5} and Daniel A Charlebois^{2,3,*}

¹ Department of Mathematical and Statistical Sciences, University of Alberta, 11455 Saskatchewan Drive NW, Edmonton, Alberta, Canada

² Department of Physics, University of Alberta, 11455 Saskatchewan Drive NW, Edmonton, Alberta, Canada

³ Department of Biological Sciences, University of Alberta, 11455 Saskatchewan Drive NW, Edmonton, Alberta, Canada

⁴ Current address: Department of Mathematics, Simon Fraser University, 8888 University Drive, Burnaby, British Columbia, Canada.

⁵ Equal contribution.

* Author to whom any correspondence should be addressed.

E-mail: dcharleb@ualberta.ca

Keywords: demography-dispersal trade-off, fungal mat, phenotypic evolution, *Saccharomyces cerevisiae*, stochastic spatiotemporal population dynamics, range expansion

Abstract

Fungi expand in space and time to form complex multicellular communities. The mechanisms by which they do so can vary dramatically and determine the life-history and dispersal traits of expanding populations. These traits influence deterministic and stochastic components of evolution, resulting in complex eco-evolutionary dynamics during colony expansion. We perform experiments on budding yeast strains genetically engineered to display rough-surface and smooth-surface phenotypes in colony-like structures called ‘mats’. Previously, it was shown that the rough-surface strain has a competitive advantage over the smooth-surface strain when grown on semi-solid media. We experimentally observe the emergence and expansion of segments with a distinct smooth-surface phenotype during rough-surface mat development. We propose a trade-off between dispersal and local carrying capacity to explain the relative fitness of these two phenotypes. Using a modified stepping-stone model, we demonstrate that this trade-off gives the high-dispersing, rough-surface phenotype a competitive advantage from standing variation, but that it inhibits this phenotype’s ability to invade a resident smooth-surface population via mutation. However, the trade-off improves the ability of the smooth-surface phenotype to invade in rough-surface mats, replicating the frequent emergence of smooth-surface segments in experiments. Together, these computational and experimental findings advance our understanding of the complex eco-evolutionary dynamics of fungal mat expansion.

1. Introduction

Yeast exist in microbial communities that interact with their environment and expand over time and space to form complex multicellular populations that can display intricate patterns. This spatial organisation has a profound impact on the dynamics and evolution of expanding yeast communities. Many examples exist of how the spatial structure, absent in well-mixed experiments, can affect evolutionary dynamics [1–3]. In particular, spatial structure can result in a unique stochastic phenomenon known as ‘allele surfing’, where mutations occurring at the

outer boundary of an spatially expanding population can travel along the advancing front and are more likely to reach higher frequencies [4–7]. Some of the most striking and early experimental evidence of allele surfing was observed by Hallatschek *et al* using fluorescently-labelled strains of otherwise genetically identical bacteria. They observed distinct monoclonal segments emerge as initially well-mixed colonies expanded [6]. Under selection, allele surfing can serve to accelerate the spread of beneficial mutations, or lead to an ‘expansion load’, where deleterious mutations surf to higher frequencies than they otherwise could in well-mixed growth conditions [8]. In

term of colony growth, segments of deleterious mutations can form from allele surfing, but will generally not be able to permanently establish [9]. By contrast, beneficial mutations are able to establish large, triangular segments.

While the shape of a mutant segment reflects the selective advantage of a mutant, the number of segments that emerge reflects the competition between selection and strong genetic drift in the pioneer population. Previous experimental work found differences across species, strains, and environmental conditions in the strength of genetic drift during colony growth [10]. These experimental observations are supported by previous theoretical work, which highlights two classes of traits influencing allele surfing events: demography and dispersal traits. Demography traits are those associated with the reproductive success of an individual, including its rate of reproduction and its competitive ability in high-density environments [11]. Dispersal, meanwhile, refers to mechanisms of spatial displacement. Using a 2D stepping-stone model, Klopstein *et al* showed the role of demography and dispersal traits in determining the surfing probability of a neutral allele [4]. Their results showed that both the ability to grow at high densities and the amount of dispersal were negatively correlated with the probability of successful surfing events. This was later expanded upon to consider deleterious and beneficial mutations [5]. Simulations predicted that beneficial mutations were more likely to surf when density was limited, while deleterious mutations surfed most often when populations were able to grow at high densities. Surfing probability decreased with increasing dispersal rates for deleterious mutations, while probabilities increased with dispersal rates for beneficial mutations.

Demography and dispersal traits not only drive evolutionary dynamics, but are themselves subject to selection. Classic eco-evolutionary theory holds that at density equilibrium, high competitive ability confers a fitness advantage due to high population densities [12]. However, this process is disrupted by the introduction of spatial structure, where population density will differ between the core and edge of the population [13]. Range expansion is also associated with the evolution of dispersal traits. Spatial sorting is the process by which natural selection along the expanding population front favours individuals with higher rates of dispersal or migration [13–16]. One interesting outcome of spatial sorting is that it can result in a population less fit than would otherwise be expected in a well-mixed environment [17]. This is due to the fact that ecological traits are often subject to trade-offs; the selection of one trait comes at the cost of another.

Deforet *et al* demonstrated this phenomenon in the context of a trade-off between migration and intrinsic growth rate in bacterial colonies [13]. They derived an analytical relationship for how much cost a mutant can incur to its growth rate in favour of higher dispersal before it can no longer invade a resident population. Additionally, they experimentally observed that bacterial populations with higher dispersal consistently out-competed those with higher growth rates. Trade-offs complicate our understanding of selection, as they require balancing the advantages and disadvantages of maximizing beneficial traits over others. This is especially true for demography and dispersal traits, where which a trait's fitness advantage is not constant, but varies according to ecological factors such as population density and allele frequency [13, 18–20]. Theoretical work has predicted that evolution will select for higher growth rates and dispersal rates during the expansion of a genetically-heterogeneous population, at the cost of decreased capacity for growth at high densities along the range front [18]. However, simulations also predicted that when the evolving population was forced to compete with a resident population, selection for growth as higher densities increased. Until recently, the selective dynamics of demography and dispersal traits and their impact on allele surfing have remained two separate areas of research. However, recently Urquhart–Cronish *et al* used a one-dimensional stepping-stone simulation to study surfing of demography traits themselves [21]. They found that surfing of alleles associated with competitive ability, or an individual's capacity to grow at high densities, was more frequent. Meanwhile, the strong selection for high growth rate along the population edge reduced surfing for that trait.

The unique spatial organisation of yeast populations make them well-suited to studying eco-evolutionary feedbacks in the evolution of demography and dispersal traits during range expansion. One example of a yeast community is a fungal mat, which is a colony-like structure that requires the expression of the cell surface flocculin gene *flo11* to form [22–25]. *flo11* is responsible for the synthesis of the *Flo11* adhesin protein, which mediates surface attachment and pattern formation in yeast colonies and mats [26, 27]. *Flo11* is also required for pseudohyphae formation and invasion [22], and it interacts with drug efflux pumps and the extracellular matrix to form biofilms in the budding yeast *S. cerevisiae* [28]. Previously, colonies of *S. cerevisiae* cells with a functional copy of the *flo11* gene (i.e. a 'wild-type' strain called TBR1 with a rough-surface, pattern-forming mat phenotype) were found to grow faster and to larger sizes compared to the corresponding *flo11* knockout strain (i.e. a mutant strain called TBR5 with a smooth-surface mat phenotype) [26].

In competition assays on semi-solid agar plates, wild-type TBR1 cells outcompeted knockout TBR5 cells. The *Flo11* adhesin protein was found to constrain TBR1 mats to grow in two dimensions (2D) along the agar surface, in contrast with TBR5 mats, which grew in an unconstrained manner in three dimensions (3D). This phenomenon resulted in rapid radial expansion, which allowed TBR1 cells to push ahead of TBR5 in mat expansion. In well-mixed liquid-media experiments, no such difference in the growth of TBR1 compared with TBR5 was observed [26]. Together, these results suggest that the traits associated with the competitive advantage are unique to the spatial structure of the mats.

We propose that the rough-surface TBR1 and the smooth-surface TBR5 phenotypes are subject to a demography-dispersal trade-off. While TBR5 exhibits less spread, its capacity to grow upward allows for more growth at high densities. In contrast, TBR1 is constrained to grow in 2D, allowing it to spread more quickly but preventing it from accumulating at high densities. The previously observed advantage of TBR1 over TBR5 during competition is consistent with the theory of spatial sorting, where evolution selects for the higher-dispersing rough-surface strain [13–17]. To investigate the effects of demography-dispersal trade-offs in the spatiotemporal dynamics of yeast mat development and evolution, we performed experiments on genetically-engineered, mat-forming *S. cerevisiae* strains under ideal growth conditions to obtain the spatial distribution of a smooth-surface mutant invading an established rough-surface mat. We observed that smooth-surface segments formed on agar plates seeded with the rough-surface TBR1 strain; these smooth segments either expanded or were enveloped by TBR1. We propose that these segments are evidence of an allele surfing events. Next, we implemented a modified stepping-stone model and found that the trade-off between the ability for upward growth and the ability for outward growth in the two phenotypes explains experimental observations and generated predictions on the ability of a rough-surface mutant to invade a smooth-surface resident population. These experimental observations and theoretical predictions shed new light on our understanding of the interaction between stochastic allele surfing events and eco-evolutionary dynamics, and on how these interactions shape the genetic makeup of expanding fungal mats.

2. Materials and methods

2.1. Simulation framework

The spatiotemporal dynamics of yeast mat expansion were modelled using a variation of the stepping-stone model [9, 30–32] on a 2D lattice with a Moore

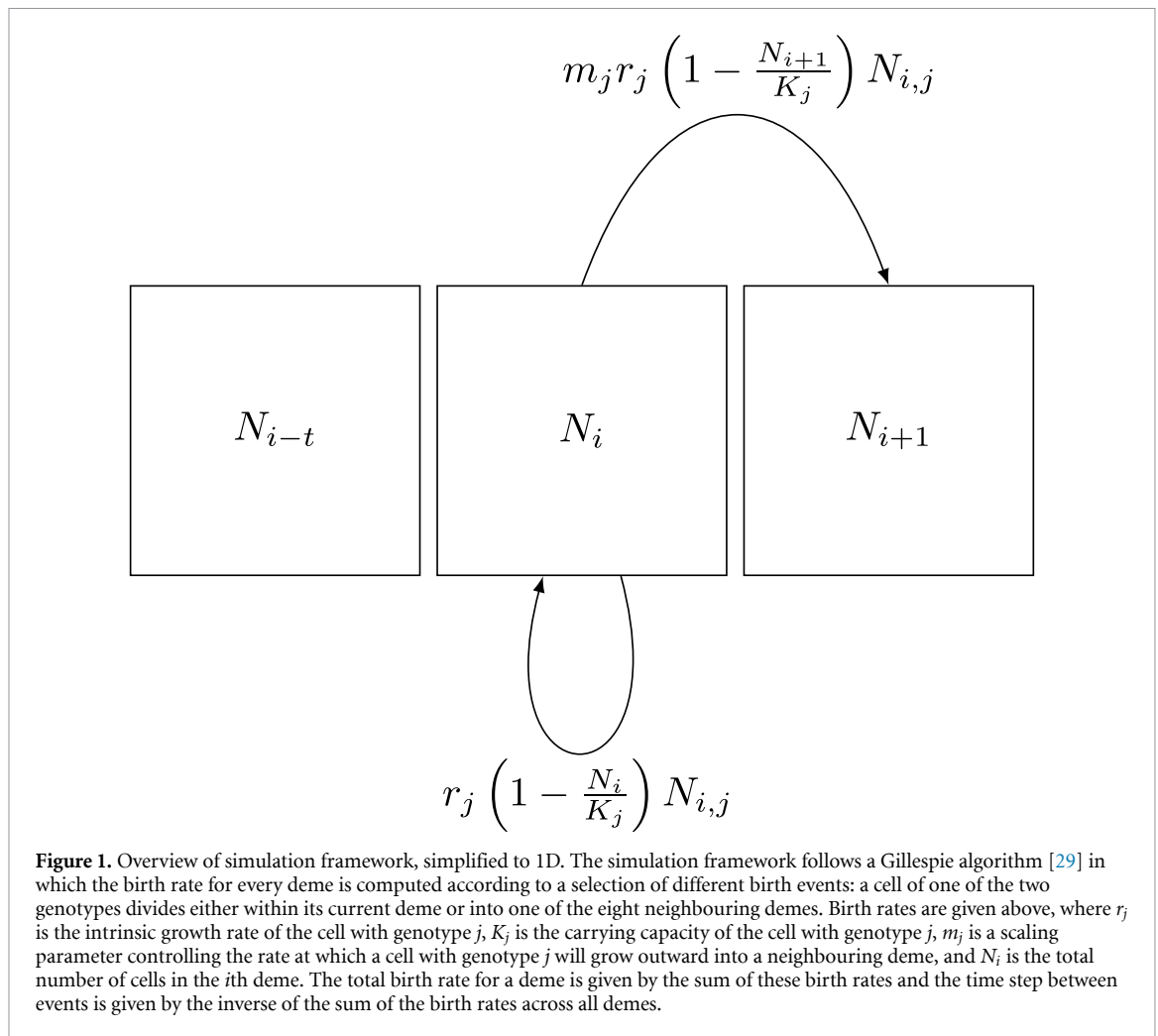
neighbourhood (i.e. the eight lattice sites surrounding a cell). Here, each lattice site represents a group of cells, called a ‘deme’. Although originally presented as a model for short-range migration between patchy populations, this model can approximate the behaviour of a continuous population when deme sizes are small relative to the total population, and has been used previously as a model for microbial colony growth [30]. As yeast cells are non-motile, cells could not migrate but rather spread to neighbouring demes via cell division. The likelihood of such a division outward corresponds to the amount of dispersal in that cell population. Reaction rates were modelled using the logistic growth equation [33] and were determined by three parameters: the intrinsic growth rate (r), the carrying capacity for the population within a single deme (K), and an expansion rate parameter (m) that scales the rate at which cells divide into a neighbouring deme. A schematic of the simulation framework simplified to one dimension (1D) is shown in figure 1. In the case of $\tilde{m} = \frac{1}{8}$ (i.e. $8\tilde{m} = 1$), then a cell surrounded by eight demes containing the same number of cells as its current deme is just as likely to reproduce outward as it is to divide into its own deme. This is described by:

$$r \left(1 - \frac{N}{K}\right) N = \sum_{i=1}^8 \tilde{m} r \left(1 - \frac{N_i}{K}\right) N,$$

where N is the population size of the current deme and N_i , $i \in [1, 8]$ are the population sizes of the surrounding demes. Therefore, expansion rates holding values in the range of $0 < m < 0.125$ make reproduction into surrounding demes less likely than reproduction within a cell’s current deme.

To model the difference between the rough-surface phenotype and the smooth-surface phenotype, we introduced a trade-off between K and m . TBR1 cells with a rough-surface phenotype have been shown to expand more rapidly and grow close to the agar surface, while TBR5 cells with a smooth-surface phenotype more readily grow upward [26]. Therefore, we modelled rough-surface cells as having a lower carrying capacity but a greater rate of expansion, while smooth-surface cells were given a high carrying capacity but a smaller rate of expansion. For simulations which considered the mutation from a cell of one type to the other, a mutation rate was introduced (see appendix A for details). During each cell division event, a cell was allowed to mutate according to the probability set by the mutation rate. In all cases, mutations could occur in either direction to reflect the high ‘evolvability’ of *flo11* [34, 35].

Simulations were initiated with 1000 demes in a center disk, each containing ten cells. The proportion of cells of each type in the demes varied for different simulation cases. Demes were coloured according



to the frequency of the cell strains present, using a gradient from white to red. Whenever the rough- and smooth-surface phenotypes were being compared, white was used to represent the rough-surface phenotype and red was used to indicate the smooth-surface phenotype. Simulations were coded in Python, which is available on github [36], and run on the Cedar cluster (Digital Research Alliance of Canada).

2.2. Yeast mat evolution experiments

Haploid *S. cerevisiae* TBR1 (Σ 1278b, $\text{mat}\alpha$, *flo11*, tryp) and TBR5 (Σ 1278b, $\text{mat}\alpha$, *flo11* Δ , tryp) strains were used for the yeast mat evolution experiments. TBR1 (*flo11*) and TBR5 (*flo11* Δ) cells are isogenic apart from the presence or absence of the *flo11* gene, respectively.

TBR1 and TBR5 cells were cultured from isogenic colonies in YPD liquid medium at 30 °C and shaken overnight at 250 rpm (VWR 1585, Catalog no. 97051-680). Then 10^7 cells ml^{-1} of TBR1 or TBR5 were inoculated from a 2 μl drop onto a Petri dish (Fisher Brand, Catalog no. FB0875712) containing YPD agar. YPD media was made with 5 g of yeast extract (Sigma–Aldrich, Catalog no. Y1625), 10 g of bacto

peptone (BD, Catalog no. 211 677), 38 mg of adenine (Sigma–Aldrich, Catalogue no. D16), and 7.5 g (or a 1.5% final concentration) of agar (agar powder/flakes for agar plates: Fisher Scientific, Catalogue no. BP1423), autoclaved in 450 ml of Type 1 water, and then supplemented with glucose (Fisher Scientific, Catalog no. D16) to a final concentration of 2%.

Agar plates were incubated at 30 °C in an environmental chamber (Thermo Scientific, Catalog no. 13-067-066) at 50% humidity. Yeast mats seeded with TBR1 or TBR5 *S. cerevisiae* cells were grown for 30 days. These mats were photographed daily using a Canon EOS Rebel SL3 camera with a Canon EF-S 35 mm f/2.8 Macro IS STM macro lens.

2.3. Growth rate measurements

To determine the growth rates of the TBR1 and *tbr1* strains, rough- and smooth-surface cells respectively were extracted from TBR1-seeded agar plates using 20 μl sterile pipette tips (Fisher Scientific, Catalog no. 02-707-432). Specifically, 6 cultures of TBR1 cells with the rough-surface phenotype and 6 cultures of *tbr1* cells with the smooth-surface TBR5-phenotype were grown in liquid YPD medium for 3 d. Every 12 h,

cell counts were obtained (Corning, Catalog no. 07-201-800) and the liquid cultures were re-suspended to an initial concentration of $N_0 = 10^6 \text{ cells ml}^{-1}$ to keep cultures in the log-phase of growth. The exponential growth rate was calculated from:

$$r = \frac{1}{t_r} \ln(N(t)/N_0),$$

where t_r is the time interval between re-suspensions and $N(t)$ is the cell count at time t before re-suspension [33].

2.4. Image processing

The *tbr1* smooth-surface phenotype segments that emerged in TBR1-seeded agar plates were quantified each day from photographs. Daily *tbr1* segment counts and mat area measurements were obtained for 30 d. Quantitative analysis of the *tbr1* segments was completed based on the area fraction of the *tbr1* segments using the image processing software ImageJ [37]. The area fraction represents the ratio of the area of the *tbr1* segments to the total area of the TBR1-seeded mat. The resolution of original images was 6000 by 4000 pixels with an aspect ratio of 3:2. These original images were cropped to a square ratio (1:1) such that the circumference of the Petri dish touch each of the 4 sides of the image. The area fractions of the segments were evaluated using the cropped images. This maintained accuracy when scaling the image pixels by the length of the Petri dish in each image, such that the area evaluation of the segments and the mat itself remained consistent throughout the analysis. Data supporting our study is available on Mendeley Data [38].

3. Results and discussion

We began by separately seeding YPD agar plates with TBR1 and TBR5 cells. In agreement with previous experimental results [26], the TBR5 mats formed with a circular, smooth-surface phenotype (figure 2(A)), whereas the TBR1 mats formed with a less circular, rough-surface phenotype (figure 2(B)). Phenotypically distinct segments emerged in approximately half of the TBR1-seeded plates as the mat expanded (figures 2(B) and C7). These segments resembled the smooth-surface phenotype of the TBR5 mats. Some of these segments formed large, triangular segments, while others were enveloped by TBR1 cells and effectively frozen in time and space (figure C3). Henceforth, we denote these phenotypically-smooth cells as ‘*tbr1*’.

One possible mechanism for the appearance of the smooth-surface segments on TBR1-seeded agar plates is that these segments represent the establishment of a mutation in the *flo11* gene. This is based on the fact that *flo11* contains tandemly repeated DNA sequences [39]; it is also known that the

number of tandem sequences in the cell can change rapidly and accelerate the evolution of coding and regulatory sequences [34, 35]. This feature gives rise to high ‘evolvability’ of *flo11* in TBR1 cells, which directly impacts the phenotype of the mat surface: a rough-surface can be attributed to a functional *flo11* gene, while a smooth-surface can be attributed to a nonfunctional (or knocked out) *flo11* gene. We hypothesise that the appearance of these smooth-surface *tbr1* segments is due to a mutation in *flo11*, which results in a phenotype similar to the TBR5 strain.

Liquid media growth rate measurement experiments revealed no significant difference between the growth rate of rough-surface, pattern-forming TBR1 cells and smooth-surface *tbr1* cells (figure 3). This is in agreement with previous experimental results on the growth rates of TBR1 cells and TBR5 cells in liquid media [26]. Together, these results support our hypothesis that *tbr1* cells are phenotypically similar to TBR5 cells. The growth rate in liquid media hovered around 0.24 per hour, which we used as the intrinsic growth rate for subsequent simulations. The establishment of a smooth-surface phenotype is of particular interest given the previous results demonstrating that TBR1 had an advantage over TBR5 cells when expanding across an agar surface [26]. The appearance of these smooth segments may be encouraged by the rough front and lower density of the TBR1 phenotype, which is likely to facilitate successful allele surfing events [10]. However, changes in the growth patterns (i.e. 3D growth of TBR5 versus 2D growth of TBR1) may also provide the smooth-surface phenotype with an initial selective advantage. This is because a necessary first step in successful allele surfing is the local accumulation of mutant cells along the population front [40]. The 3D growth of the smooth-surface cells may give them a local advantage over the rough-surface cells, thus the capacity for these cells to grow at higher densities would increase the probability that local allele frequencies are sufficiently large to surf. Additionally, previous work demonstrated that competitive ability increases in a population when it must invade a resident population [18] suggests that the ability to grow upward and at higher densities will assist the smooth-surface mutants to invade the resident rough-surface population.

To investigate these hypotheses, we simulated a modified stepping-stone model [32] (figure 1). In our model, the ability to grow upward was described by a higher carrying capacity (K), while outward growth was controlled by an expansion rate parameter (m). We first performed simulations of competition between two strains of the same phenotype. Half the initial cells were of one phenotype and half were of the other. Cells were well-mixed within demes, which correspond to small local populations [41]. Our simulations revealed that the final mat area increased with expansion rate, but did not

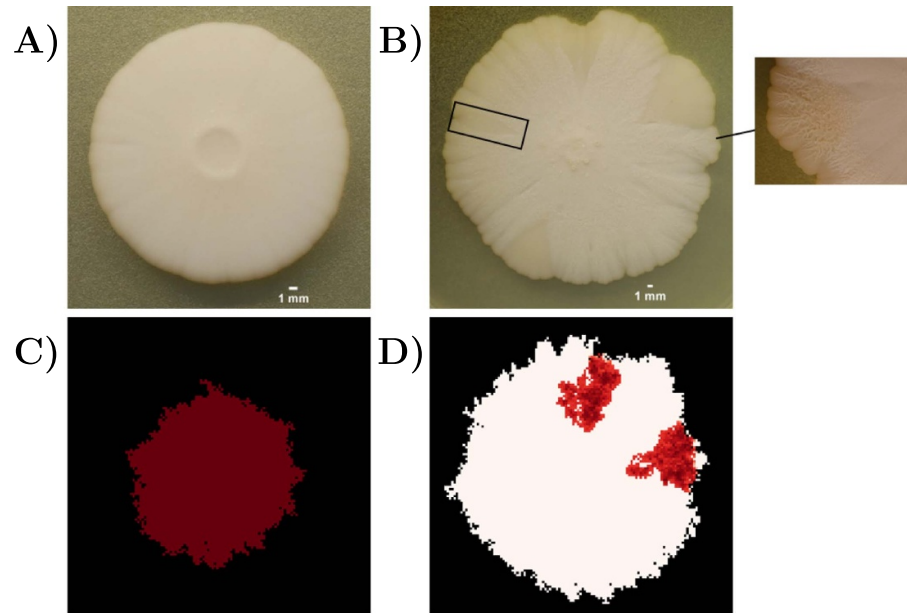


Figure 2. Experimental and *in-silico* phenotypic evolution of TBR1 and TBR5 mats. Representative images of (A) a TBR5 (*flo11Δ*) *S. cerevisiae* mat and (B) a TBR1 (*flo11*) seeded *S. cerevisiae* mat after 3 weeks of growth at 30 °C on a YPD agar plate. The inset of (B) shows the patterns that emerge on the surface of the TBR1-seeded mat. (C) Simulation of a TBR5 mat after 20 d, which is depicted in red. Parameters were as follows: $K = 90$ cells/deme, $m = 0.025$, and $r = 0.24 \text{ h}^{-1}$. Mutations were not permitted, as TBR5 cells lack the *flo11* gene. (D) Simulation over 20 d of a TBR1 mat, which was permitted to mutate into cells with a smooth-surface phenotype. Demes were coloured according to the frequency of the cell strains present using a gradient from white for rough-surface cells to dark red for smooth-surface cells. Parameters were as follows: $K_{WT} = 30$ cells/deme and $m_{WT} = 0.05$ for rough-surface cells, $K_{MT} = 90$ cells/deme and $m_{MT} = 0.025$ for smooth-surface cells, and $r = 0.24 \text{ h}^{-1}$ for all cells.

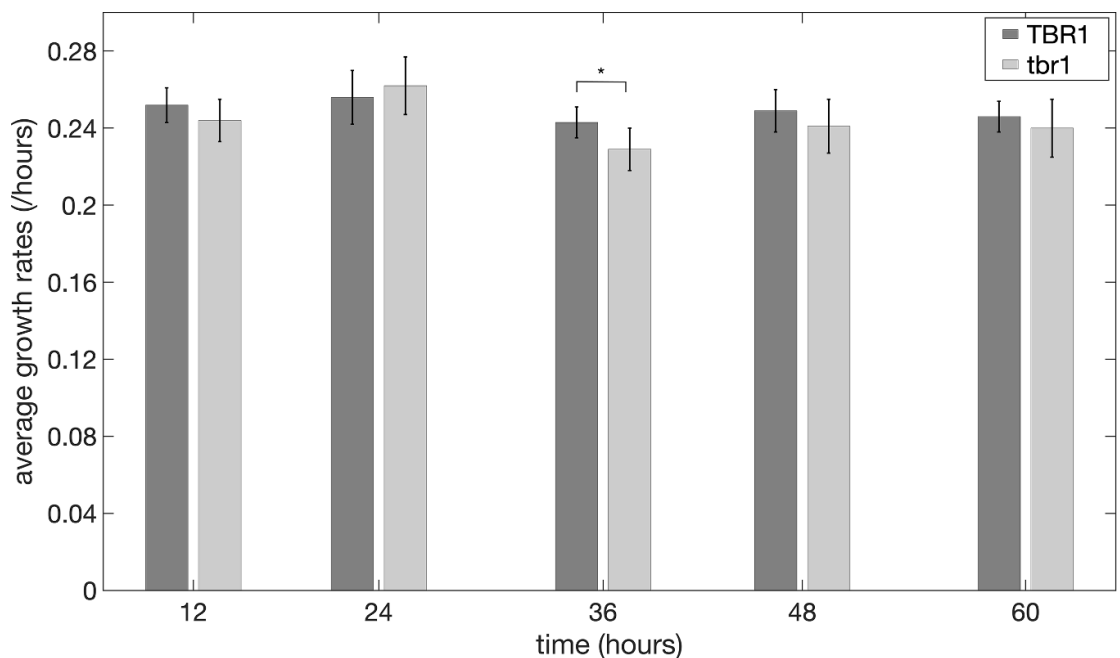


Figure 3. Average growth rates of rough-surface, pattern forming phenotype TBR1 cells and smooth-surface phenotype *tbr1* cells in liquid medium. Average growth rates were obtained approximately every 12 h for 2.5 d. An independent samples t-test was performed to compare the TBR1 and *tbr1* growth rates for a sample size of $N = 6$. No significant difference in growth rates ($p > 0.05$) was found except at 36 hours ($p = 0.03$).

depend on the carrying capacity of the extracellular environment (figure C1(A)) [26]. We also calculated the unitless P2A quantity given by $\frac{P^2}{4\pi A}$, where P is the perimeter and A is the mat area. P2A is a

measure of the irregularity of the boundary, which increases as the mat edge becomes more irregular. The final P2A of the mats increased with both carrying capacity and expansion rate (figure C1(B)).

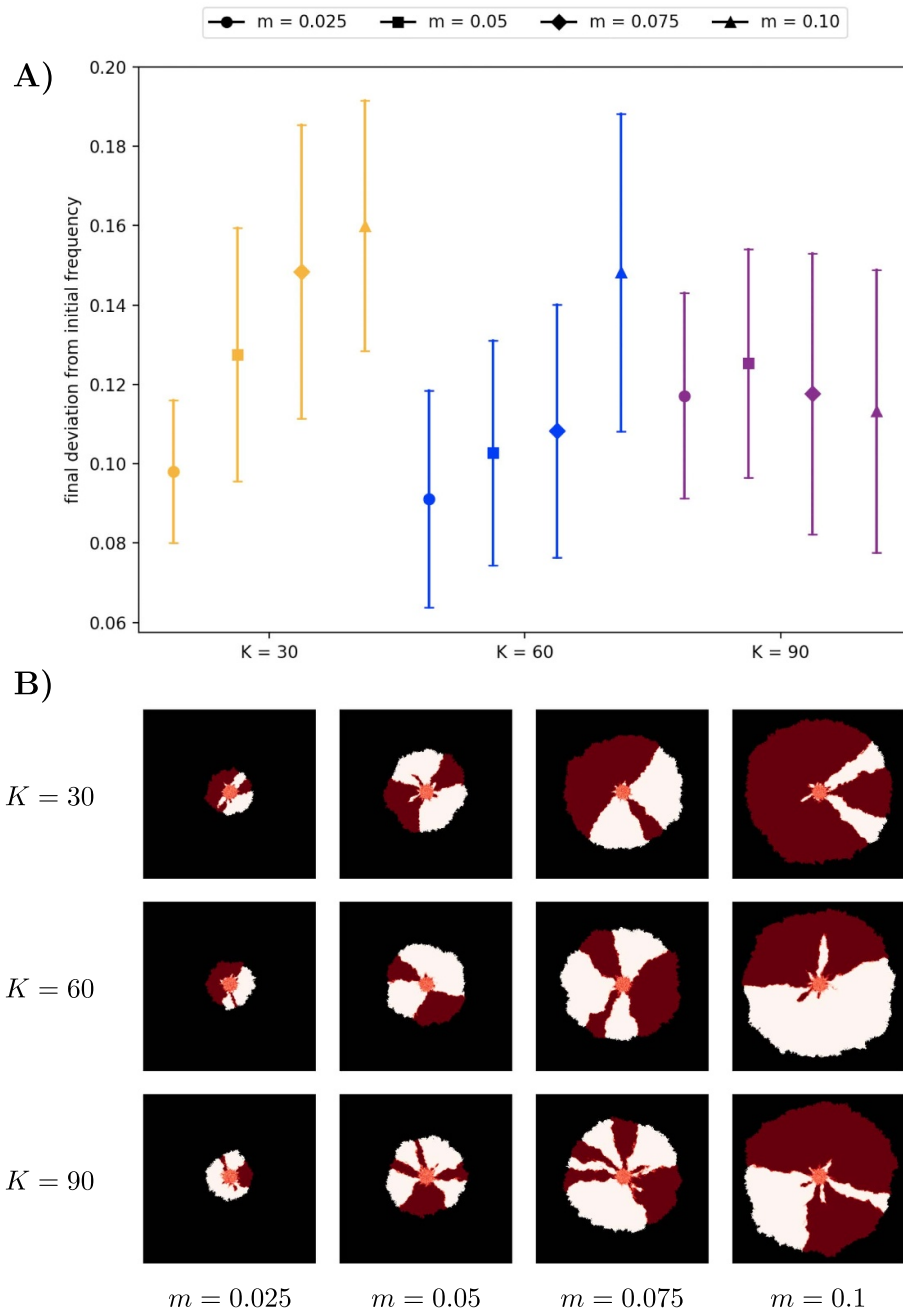


Figure 4. *In-silico* head-to-head competition between neutral mutations in mats with different carrying capacities (K) and expansion rates (m). (A) 95% confidence intervals for the mean deviation of the final mat composition from the initial frequency of 0.5 for different combinations of carrying capacity (K (cells/deme)) and expansion rate (m) parameters. (B) Images of the final simulated mats. Demes were coloured according to the frequency of the cell strains present using a gradient from white for one strain to dark red for the other strain. Mat growth over 50 d was simulated, with 30 replicates for each set of parameters. For all simulations, the lattice was seeded with a center circle of 1000 demes containing ten cells each. The initial frequency of each strain was 0.5. The final deviation from the initial frequency in (A) was calculated from the mean absolute difference between the final and initial strain frequencies, which indicates the strength of genetic drift. All cells had the same traits, with an intrinsic growth rate of $r = 0.24 \text{ h}^{-1}$. Mutation was not permitted to simulate neutral competition between the strains.

Additionally, our results showed that as expansion rates increased, so did the average amount by which the final frequency of the two strains differed from the initial frequency of 0.5. This implies that genetic drift was stronger when expansion rates were higher (figure 4(A)). However, this effect decreased as the carrying capacity increased. These observations are

indicative of the complex eco-evolutionary feedback loops between deme size, dispersal rates, and the effective population size along the range expansion front [7, 8, 11, 42]. For all parameter values, clear segments of the each cell strain formed despite neither strain having a selective advantage over the other (figure 4(B)). These results also agree with previous

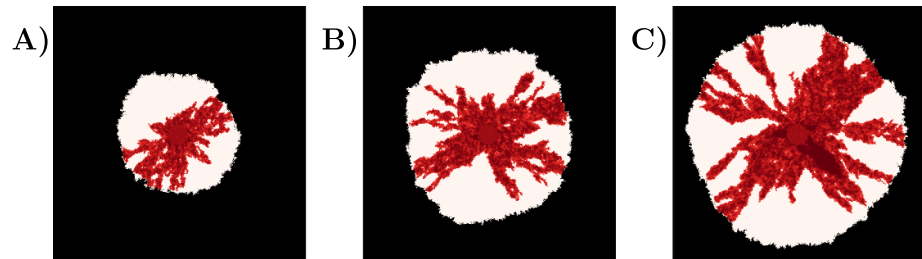


Figure 5. Representative images of simulated competition between rough-surface (WT) and smooth-surface (MT) phenotypes. Mat growth was simulated for 50 d. Carrying capacities for all three images are $K_{WT} = 30$ cells/deme and $K_{MT} = 90$ cells/deme. The intrinsic growth rate for all cells was $r = 0.24 \text{ h}^{-1}$. Expansion rate parameters increase from left to right as follows: (A) $m_{WT} = 0.05$ and $m_{MT} = 0.025$, (B) $m_{WT} = 0.075$ and $m_{MT} = 0.05$, and (C) $m_{WT} = 0.10$ and $m_{MT} = 0.075$. Demes were coloured according to the frequency of the cell strains present, using a gradient from white for smooth-surface cells to dark red for rough-surface cells.

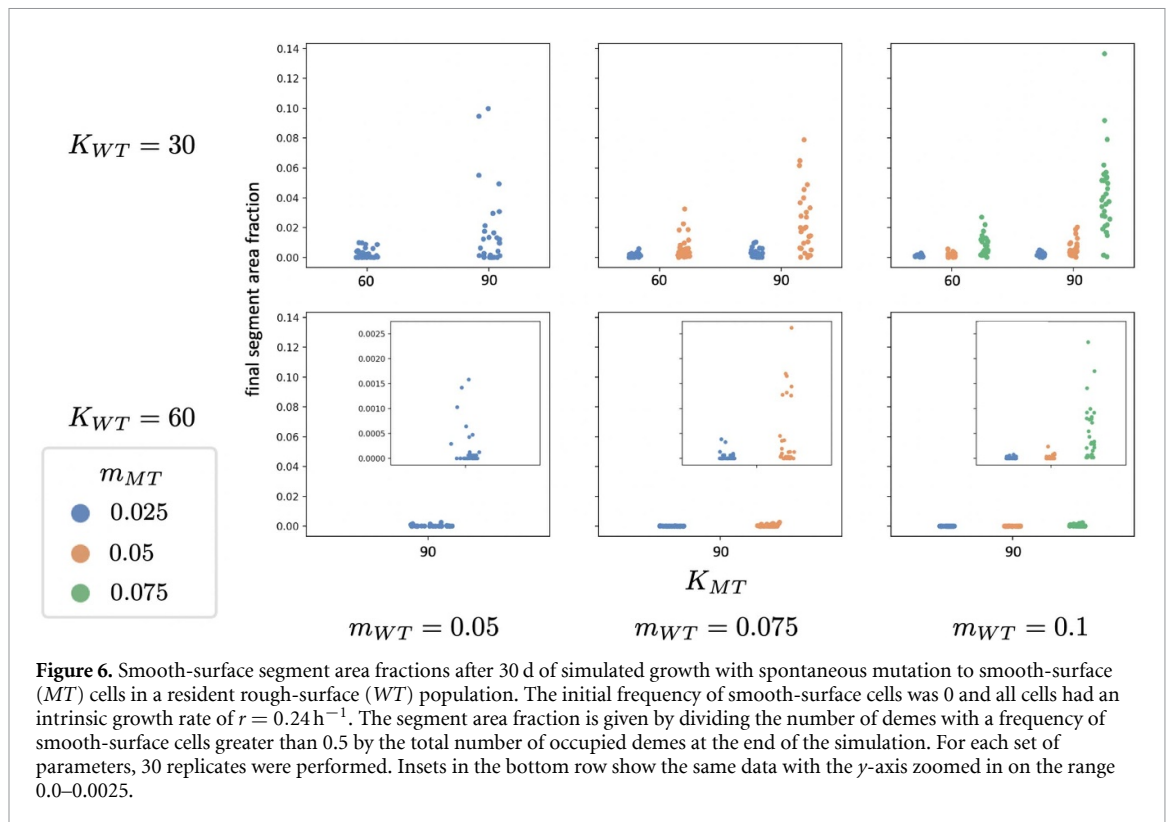
theoretical and experimental work on allele surfing and segregation of neutral mutations during microbial range expansion [6, 30, 31, 43].

We then compared our model to previous experimental results by simulating competition between the rough-surface phenotype with a higher expansion rate and the smooth-surface phenotype with a higher carrying capacity. In all cases, the rough-surface phenotype out-competed the smooth-surface phenotype (figures 5, C2 and table D1). This is evidenced by the fact that the final mean frequency of smooth-surface cells decreased from the initial frequency of 0.5 for all parameter values. The final mean frequency of smooth-surface cells was lowest (as low as 0.0074) when the carrying capacities of the smooth- and rough-surface cells were similar and the expansion rate of the rough-surface strain was large relative to that of the smooth-surface strain, which indicated that the rough-surface strain had the greatest advantage over the smooth-surface strain at these parameter values (table D1). As the carrying capacity of the smooth-surface strain became larger relative to the rough-surface strain (i.e. its competitive advantage increased) or the growth advantage of the rough-surface strain decreased, the final mean frequency of the smooth-surface strain was larger. In these cases, the net advantage of the rough-surface strain over the smooth-surface strain was less, however the mean frequency of smooth-surface cells still fell below 0.4 for all parameter sets considered. The final mat images showed that rough-surface segments formed larger triangular segments and often enveloped smooth-surface segments (figure 5). These results are qualitatively in agreement with previous experimental findings [26], where rough-surface TBR1 cells had a competitive advantage over smooth-surface TBR5 cells in agar-plate competition assays. This suggests that the advantage of TBR1 on semi-solid media can be explained by a demography-dispersal trade-off.

To understand how a demography-dispersal trait trade-off might play a role in the emergence of smooth-surface segments in TBR1-seeded plates, we simulated the growth of mats with mutation. We

first simulated mats seeded with only a rough-surface cell strain. At each cell division, we probabilistically allowed a rough-surface cell to mutate to a smooth-surface cell (see appendix A for details). Mat growth was simulated over 30 d as in our experiments. We observed the successful establishment of segments, resembling our experimental results (figure 8). This establishment was most frequent as K and m of the smooth-surface cells increased (figure 6 and table D2), due to their increased overall fitness. Segments were also more likely to establish when the carrying capacity of the rough-surface cells was smaller, regardless of whether the difference between the carrying capacities of the rough- and smooth-surface cells was the same (e.g. $K_{WT} = 60$ cells/deme and $K_{MT} = 90$ cells/deme versus $K_{WT} = 30$ cells/deme and $K_{MT} = 60$ cells/deme in figure 6). Additionally, while the frequency of large segments establishing decreased as the expansion rate of the rough-surface cells increased relative to that of the smooth-surface cells, if both expansion rates were increased while maintaining the same difference between them, larger segments established more often (e.g. $m_{WT} = 0.05$ and $m_{MT} = 0.025$ versus $m_{WT} = 0.075$ and $m_{MT} = 0.05$ or $m_{WT} = 0.1$ and $m_{MT} = 0.075$ in figure 6). This corresponds to the observations of genetic drift during competition of two neutral strains (figure 4), where larger expansion rates led to increased drift. Therefore, a likely explanation for this difference in segment area is an increase in stochastic effects such as genetic drift and allele surfing. Final frequencies show the same trends as final segment area fractions (figure C4 and table D2).

We then asked if the trade-off between local growth and expansion rate would result in different invasion dynamics when rough-surface cells are the mutant in a resident population of smooth-surface cells. Head-to-head competition showed that the rough-surface phenotype only showed a competitive advantage after a sufficient number of cells had established [26]. Considering our trade-off hypothesis, this raises the question of whether the lower carrying capacity of the rough-surface cells results in

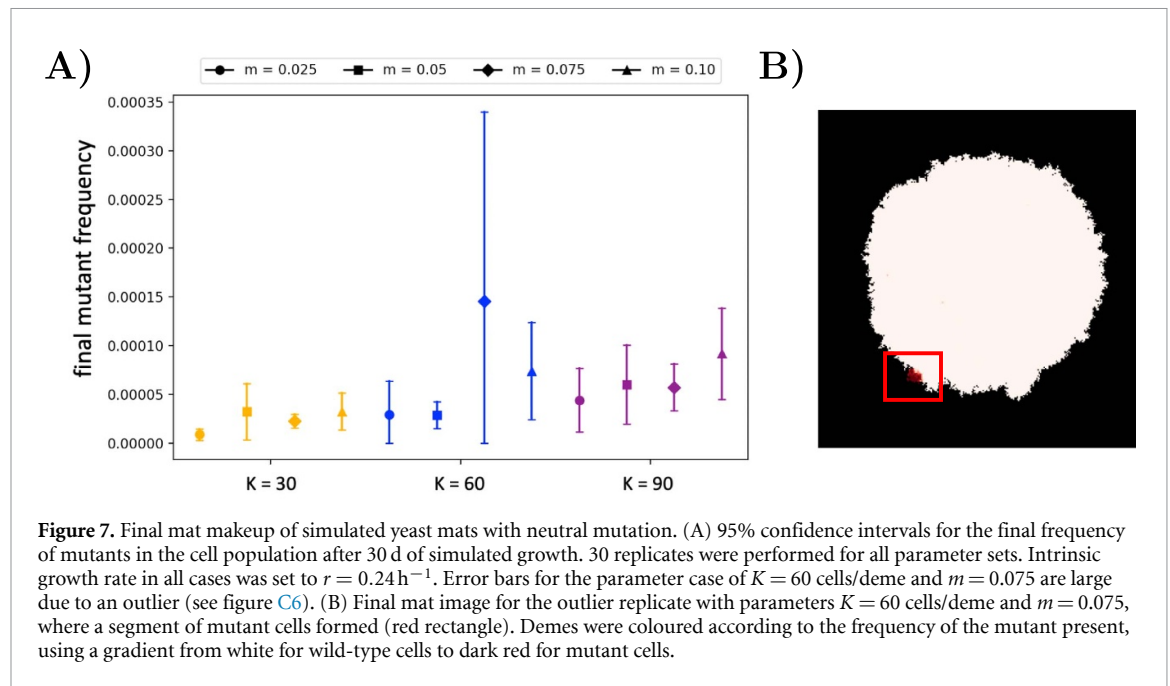


a disadvantage when these cells are sufficiently rare, as the smooth-surface cells may locally outcompete the rough-surface cells before they have the opportunity to spread. Additionally, as shown in figure 4(A), the different carrying capacity and expansion rate of the smooth-surface cells will change the strength of genetic drift during mat growth, potentially resulting in fewer allele surfing events. To investigate to what extent the demography and dispersal traits of the resident and mutant populations determine the evolution of the mat, we ran simulations of mats seeded with smooth-surface cells which were allowed to mutate rough-surface cells.

Segments of rough-surface cells did not successfully establish in the majority of mats across all parameter values (figure C5 and table D3). When segments did establish, they formed in cases when the carrying capacities of both the rough- and smooth-surface cells were low. Notably, segments only established when the expansion rate of the resident smooth-surface cells was sufficiently large (greater than 0.05). This phenomenon can also be attributed to the stronger genetic drift experienced by mats with greater expansion rates. The lack of successful rough-surface segment formation in smooth-surface mats in our simulations supports our hypothesis that the demography-dispersal trade-off between the rough- and smooth-phenotypes gives the high carrying capacity smooth-surface phenotype a fitness advantage at low frequencies, despite the disadvantage it incurs at high frequencies due to its diminished dispersal. For segments of rough-surface cells to

form in smooth-surface mats, these cells must reach a sufficiently high frequency in the population via chance effects in order to achieve the advantage conferred by higher dispersal and continue to invade. However, when rough-surface cells do successfully establish, their dispersal advantage allows these segments to increase their frequency and expand their area fraction (figure C5) past the visibility threshold (i.e. the minimum area fraction necessary to visualise a segment; appendix B).

Simulation results for spontaneous mutations in rough- and smooth-surface mats indicate the role of stochasticity in segment formation. To better quantify the effects of genetic drift, we considered the neutral-mutation cases: mats were allowed to mutate, but traits of the mutants did not differ from the wild type. Across all parameter values, segments failed to pass the visibility threshold (figure C6). In one case, a segment with a high concentration of mutant cells began to form near the end of the 30 d (figure 7(B)). The extent of its segregation from the pioneering population suggests it might have successfully reached the threshold given an extended simulation time. Although the mutant population rarely became visible, the final frequencies of mutant cells did increase with both carrying capacity and expansion rate (figure 7(A)), indicating a greater number of allele surfing events. Increased drift from increased expansion rate is in agreement with the neutral competition results in figure 4(A). However, the effect of carrying capacity on mutations differs from its effect on neutral competition in simulations. While



the relationship between the strength of genetic drift during neutral competition and the size of the carrying capacity reflected feedback loops with the expansion rate, the effects of carrying capacity on mutational success were less complex: as carrying capacity increased, so did the success of neutral mutations.

Our results indicate that some selection is necessary for segments to form from a single mutation. In the case of smooth-surface cells invading the rough-surface cells, this comes in the form of a higher carrying capacity increasing the likelihood of initial establishment. On the other hand, rough-surface cells relied on chance events to establish an initial population similarly to the neutral mutations. For parameter sets where no visible segments formed, the mean final allele frequency of the rough-surface cells amidst smooth-surface cells was often an order of magnitude less than the mean final allele frequencies of neutral mutants (tables D3 and D4), suggesting a fitness disadvantage for rough-surface cells at low frequencies. However, unlike neutral mutants, the higher dispersal of rough-surface cells allowed them to take advantage of allele surfing events to form visible segments.

4. Conclusion

In fungal mat evolution experiments, we found that *tbr1* segments which phenotypically resembled the smooth-surface TBR5 strain of *S. cerevisiae* emerged in rough-surface TBR1-seeded mats. The emergence of the *tbr1* segments can likely be attributed to a mutation in the *flo11* gene that results in a loss of functionality of the *Flo11* adhesin protein [34]. This, together with previous competition experiments establishing that TBR1 mats have a fitness advantage over TBR5 mats on semi-solid media [26],

inspired us to investigate how the appearance of the smooth-surface segments may be attributed to differences in the growth patterns influencing natural selection and the frequency of allele surfing events.

We propose that there exists a demography-dispersal trade-off in the fungal communities of TBR1, *tbr1*, and TBR5 strains, whereby rough-surface cells have a high rate of expansion but a small local carrying capacity, while smooth-surface cells have a low rate of expansion but a large local carrying capacity. Using a modified 2D stepping-stone model, we found that such a trade-off explained the competitive advantage of rough-surface cells over smooth-surface cells during yeast mat expansion. Our model also captured the appearance of smooth-surface segments in rough-surface mats resulting from spontaneous mutation (figure 8). We compared this finding to simulations of mutations of rough-surface cells in smooth-surface mats, along with simulations of neutral mutations, and found that the higher local carrying capacity of the smooth-surface phenotype was necessary for segments to establish. Our simulations further demonstrated that changes in these demography and dispersal traits affect the occurrence of successful allele surfing events.

Future experimental work will involve sequencing the evolved *tbr1* strain to identify genetic mutations that may underlie their smooth-surface phenotype. Additional experiments examining the invasion of TBR5 in resident TBR1 populations are required to validate our computational prediction that a small local carrying capacity hinders the establishment of the rough-surface phenotype in smooth-surface mats. Our fitness measurement of TBR1 and *tbr1* were performed in liquid medium, which is a limitation as culture conditions are known to impact

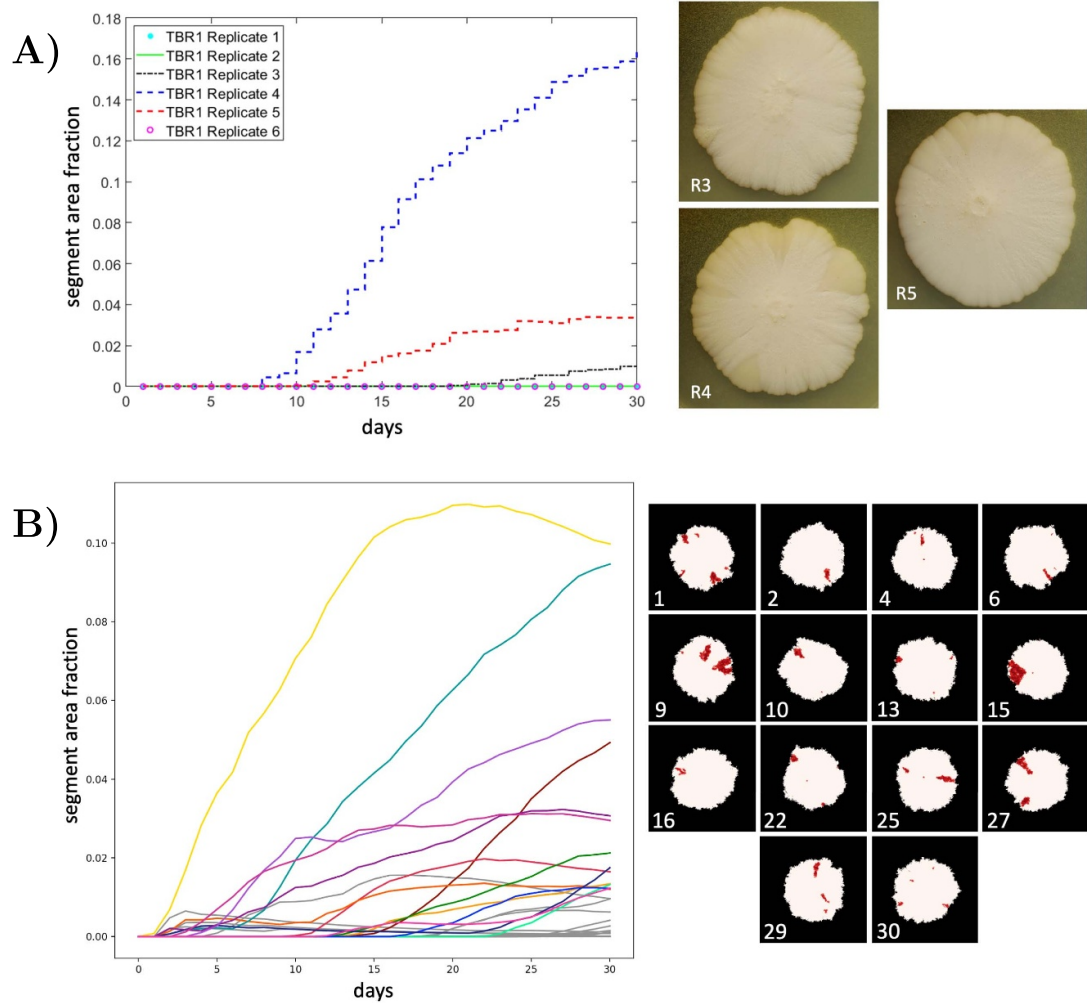


Figure 8. Experimental and *in-silico* development of rough-surface, pattern-forming TBR1 seeded mats. (A) Experimental area fraction of *tbr1* smooth-surface mutant segments in each replicate over 30 d. Visible smooth-surface segments established in three of the six replicates. Images of these mats at the end of the experiment are displayed on the right. (B) Simulated area fraction of the smooth-surface phenotype over the course of 30 d of simulated growth with mutation of smooth-surface (*MT*) cells in a resident rough-surface (*WT*) mat. The segment area fraction is given by dividing the number of demes with a frequency of smooth-surface cells greater than 0.5 by the total number of occupied demes. Parameters were set as follows: $K_{WT} = 30$ cells/deme, $K_{MT} = 90$ cells/deme, $m_{WT} = 0.05$, $m_{MT} = 0.025$, and $r = 0.24 \text{ h}^{-1}$. 30 simulation replicates were performed. Those that had a final area fraction above the threshold 0.01 were considered ‘visible’ and are plotted in colour. Images of these mats at the end of the simulation are shown on the right. Demes were coloured according to the frequency of the smooth-surface cells present, using a gradient from white for smooth-surface cells to dark red for rough-surface cells.

fitness (e.g. [26]); machine learning may be able to quantify growth rates from images of TBR1, *tbr1*, and TBR5 strains on semi-solid media [44]. Our model could be augmented to incorporate nutrient diffusion and depletion [45], which results in spatial heterogeneity of the resource supply and slows mat expansion due to an increasingly nutrient-depleted environment (figure C9). In contrast, the stepping-stone model assumes that the carrying capacity is constant in all demes and that cells have unlimited resources as they expand exponentially (figure C10). Finally, as the *flo11* gene is known to affect cell adhesion to the agar surface [26, 27], simulations incorporating adhesive and intercellular forces may elucidate the physical mechanisms underlying segment formation.

Demography-dispersal trade-offs are anticipated to be relevant for range expansion where non-motile cells expand through directed reproduction rather than migration. We demonstrated how a demography-dispersal trade-off may encourage successful invasion of populations which incur a fitness disadvantage at higher frequencies, thus displaying frequency-dependent selection [46, 47]. Additionally we found that local carrying capacity and expansion rate can influence allele surfing, but that allele surfing alone is not sufficient to explain the success of smooth-surface segments. Overall, this study advances our understanding of the spatiotemporal dynamics of yeast mat development and more generally how life-history and dispersal traits influence microbial evolution.

Data availability statement

The data that support the findings of this study are openly available at the following URL/DOI: <https://data.mendeley.com/datasets/xb4r9vbh7x/1>.

Python code for simulating the stepping-stone model can be found at: <https://github.com/bekahall/meta-colony-model>.

Acknowledgments

This article is dedicated to the late André T Charlebois (1953-2020). The authors are indebted to him for his assistance with the camera setup and advice on the macro photography of yeast.

The authors thank Prof. Gábor Balázs for providing the TBR1 and TBR5 strains and for guidance on sequence evolution of the *flo11* gene, Prof. Ailene MacPherson for helpful discussions on demography-dispersal modeling, and Dr. Oleksandra (Lesia) Guinn for helpful comments on a previous version of the manuscript. We also thank Harold Flohr for assistance with figures, Enoki Li for assistance with the literature review, and Joshua Guthrie for assistance with latexdiff. Finally, we acknowledge the anonymous reviewers whose critical reading of the manuscript and helpful comments improved the study.

D C was supported by funding from the Government of Canada's NSERC Discovery Grant (RGPIN-2020-04007) and Launch Supplement (DGEGR-2020-00197), the Canadian Foundation for Innovation's John R Evans Leaders Fund (CFI-40558), and the Government of Alberta's Research Capacity Program (RCP-21-008-SEG). R H was supported by a 2020 Alberta Innovates Summer Research Studentship and a 2021 NSERC Undergraduate Student Research Award. This work was completed in part with resources provided by the Research Computing Group at Simon Fraser University and the Digital Research Alliance of Canada.

Author contributions

D C and R H conceptualised the study. A B performed the yeast mat experiments. R H developed the

modeling framework and performed the simulations. R H, A B, and D C visualised and analysed the results. R H, D C, and A B wrote the manuscript. D C supervised the study.

Appendix A. Mutation rate

Mutation rates per base pair per cell division range from 10^{-10} to 10^{-9} [48]. As the *flo11* gene consist of an open 4104 base pair reading frame on chromosome IX [49], the probability of a mutation occurring in *flo11* for any given cell division event was set to $4104 \times 10^{-9} = 4.104 \times 10^{-6}$.

Appendix B. Minimum size of a mat segment

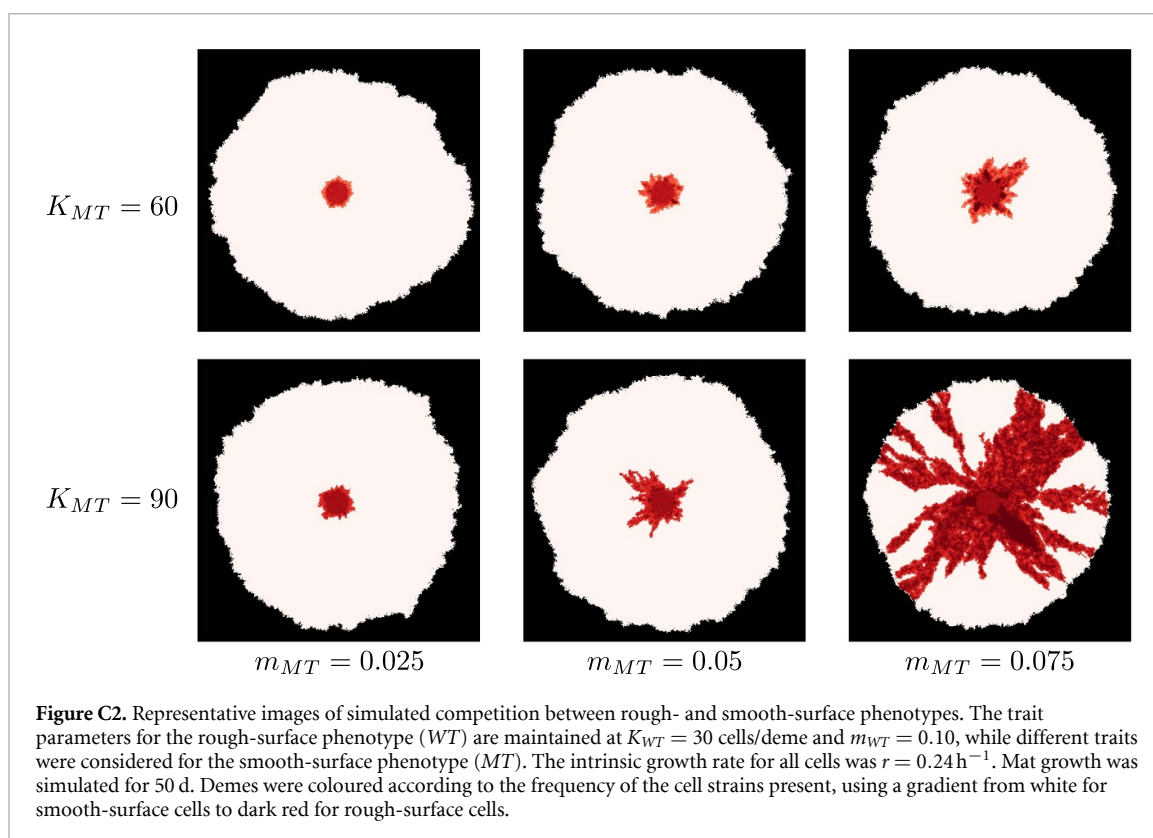
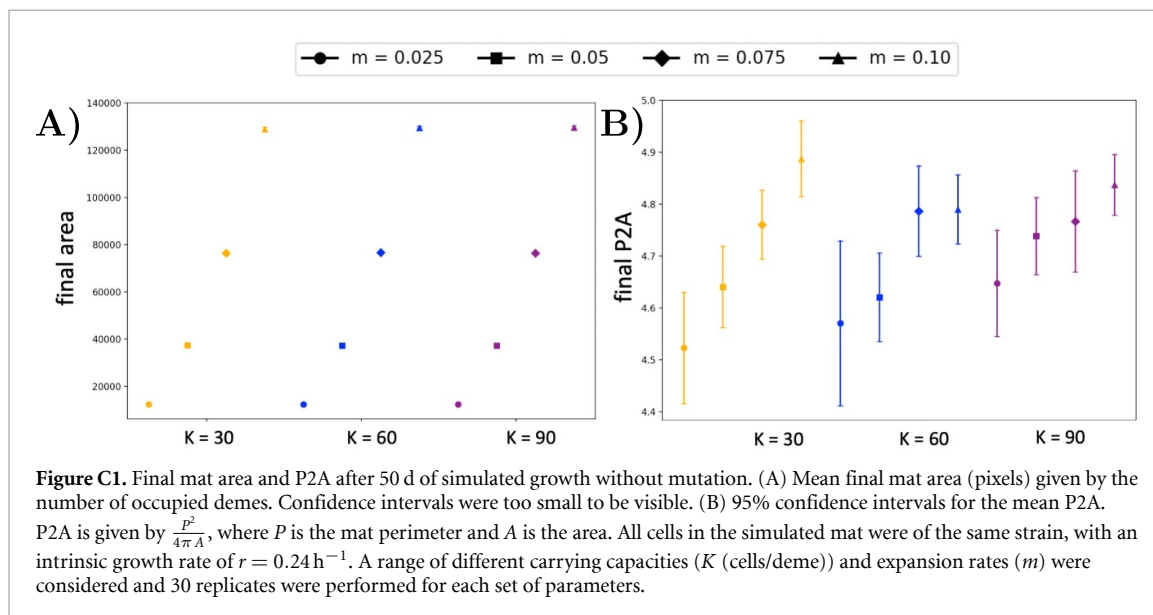
We defined the minimum dimensions of a smooth segment based on the minimum resolvable area of the naked eye. The minimum resolvable area relates to the minimum resolvable angle, which is approximately 1 arcminute (or 0.017°) [50]. This angular measurement was converted to a linear or an area measurement by considering an observer at a general viewing distance of 300 mm using the visual angle (ν) formula for angles less than 10° :

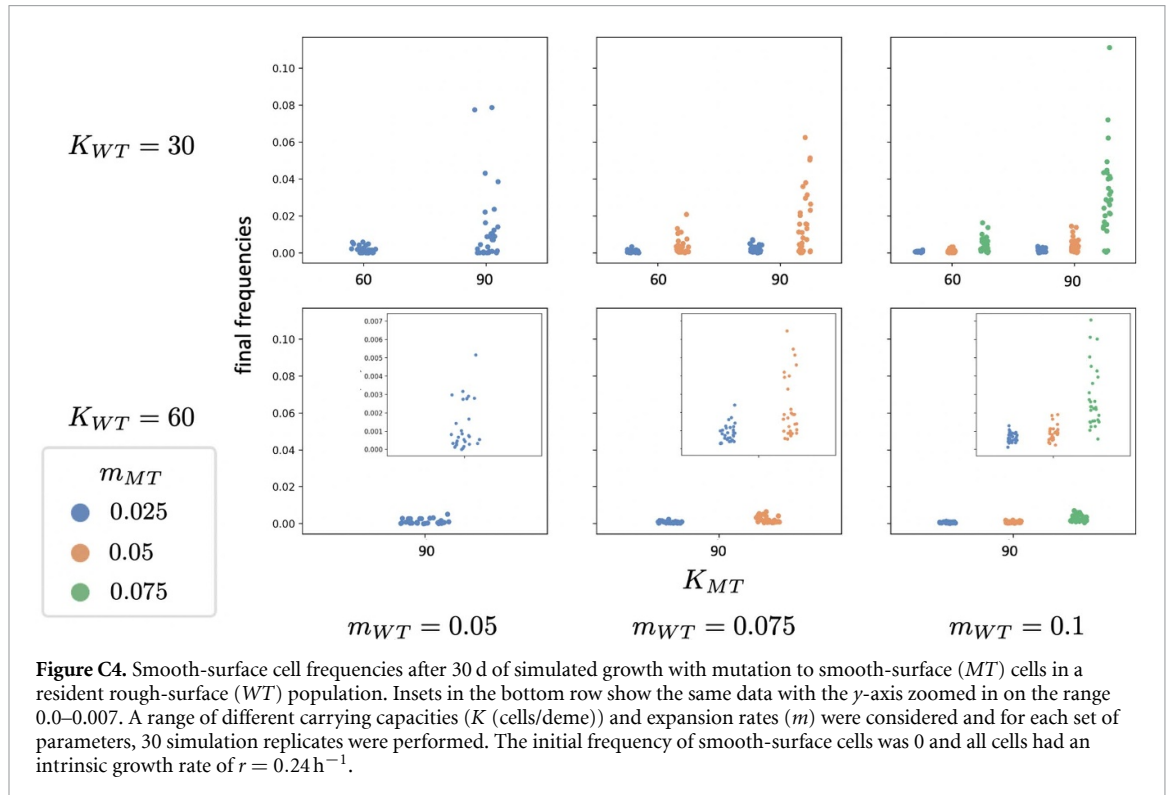
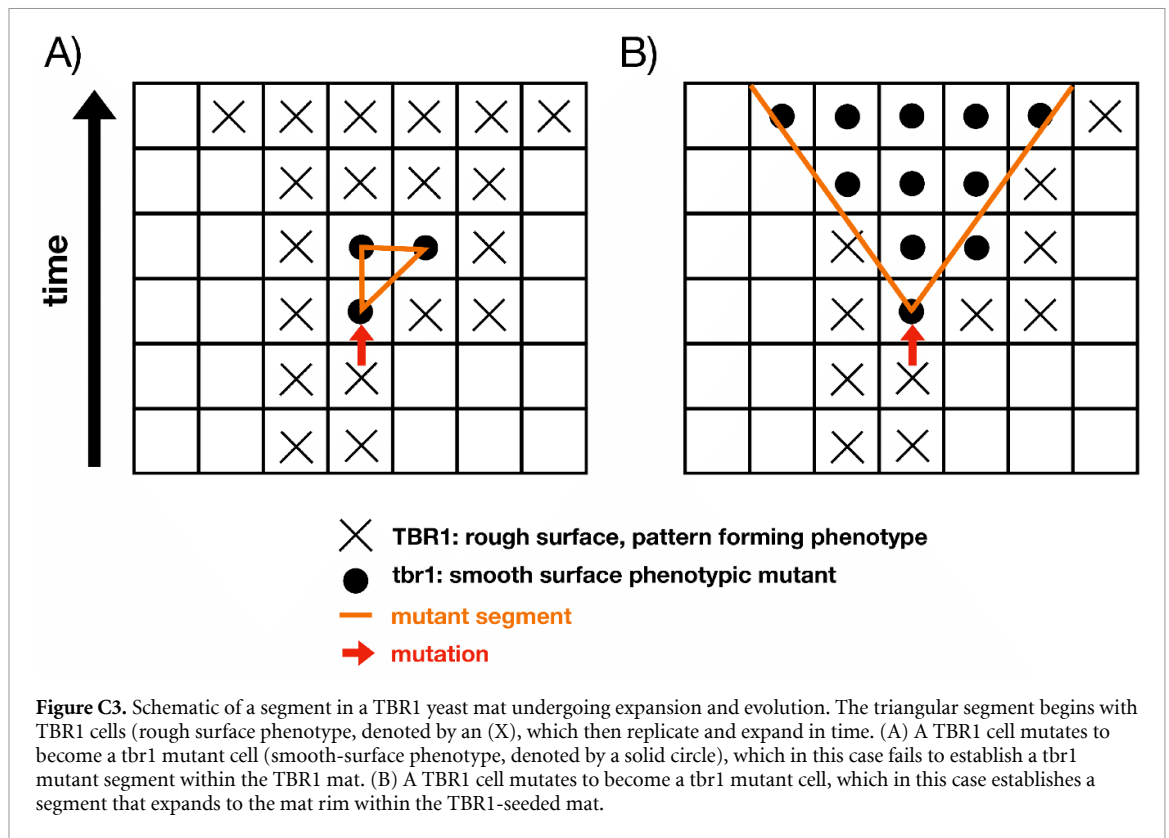
$$\tan(\nu) = \frac{\text{Minimum Resolvable Distance}}{\text{Viewing Distance}}$$

Then the minimum resolvable distance is: $\tan(\nu) \times \text{Viewing Distance} = 0.089 \text{ mm}$. Therefore the minimum resolvable area is: $(0.089)^2 \text{ mm}^2 = 0.0079 \text{ mm}^2$. The smallest smooth segment area recorded during the experiments was 0.264 mm^2 .

Due to the nature of simulations, allele frequencies and segment detection can be exact. This is in contrast to the detection of segments experimentally, which is limited by what can be detected visually. The smallest smooth-surface segment detected experimentally had a final area fraction of 0.00975 (figure 8(A)). Therefore, in our simulations we took a final segment area fraction of 0.01 as the cut-off for a visible segment (figures 8(B) and C8). When the rough-surface carrying capacity was smaller, the final segment area fraction frequently surpassed this threshold (figure 6).

Appendix C. Supplementary figures





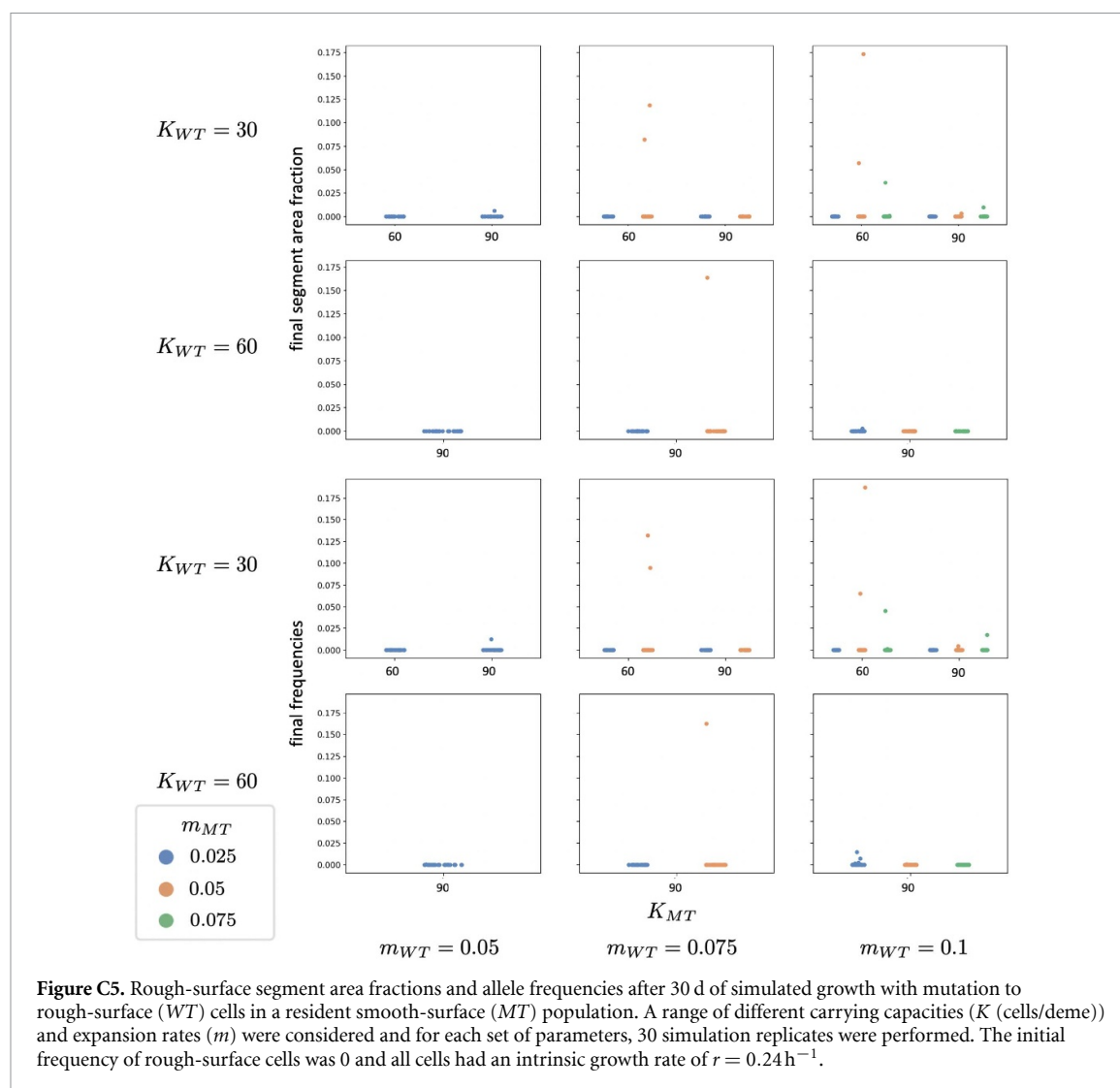


Figure C5. Rough-surface segment area fractions and allele frequencies after 30 d of simulated growth with mutation to rough-surface (WT) cells in a resident smooth-surface (MT) population. A range of different carrying capacities (K (cells/deme)) and expansion rates (m) were considered and for each set of parameters, 30 simulation replicates were performed. The initial frequency of rough-surface cells was 0 and all cells had an intrinsic growth rate of $r = 0.24 \text{ h}^{-1}$.

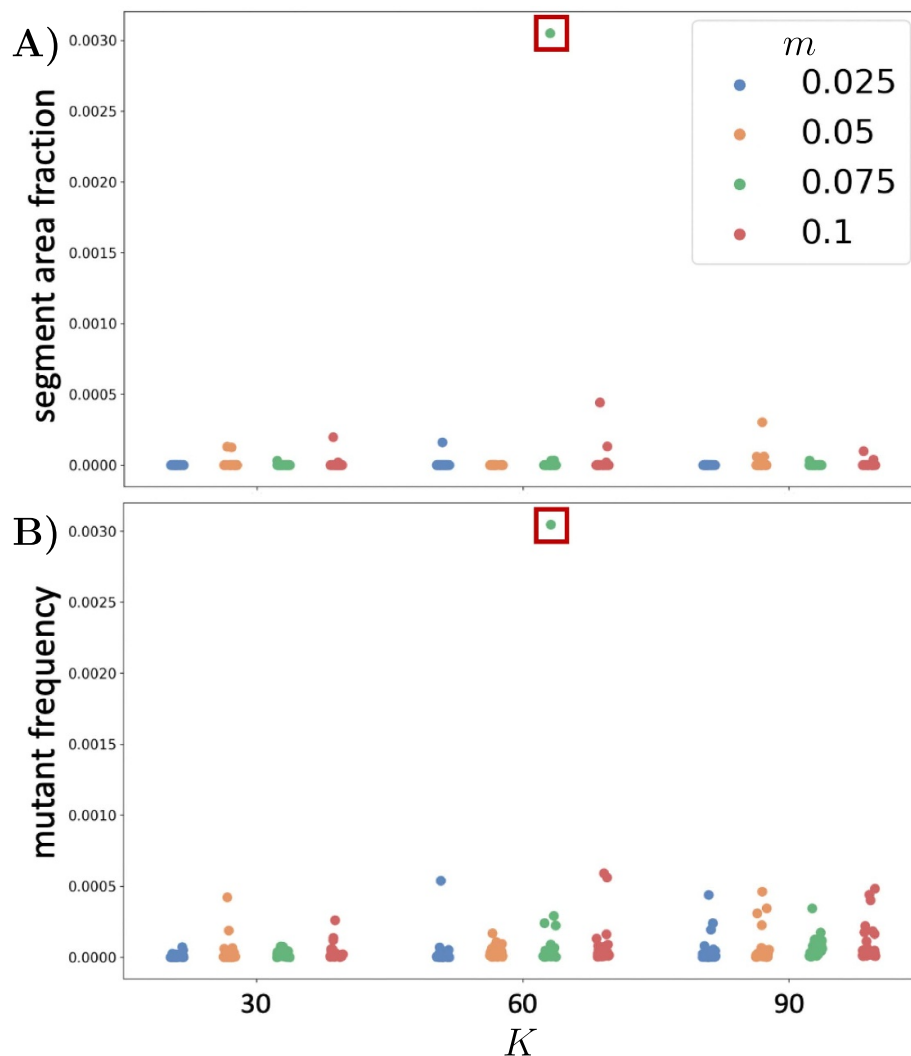


Figure C6. Final segment area fractions and frequencies after 30 d of simulated growth with neutral mutations. (A) Final fraction of the colony area consisting of mutant segments. The segment area fraction is given by dividing the number of demes with a frequency of mutant cells greater than 0.5 by the total number of occupied demes. (B) Frequency of the mutant cells throughout the whole mat. A number of different carrying capacities (K (cells/deme)) and expansion rates (m) were considered. The initial frequency of the resident population was 0 and all cells had an intrinsic growth rate of $r = 0.24 \text{ h}^{-1}$. A red rectangle highlights the area fraction and mutant frequency for the mat shown in figure 7(B). 30 simulations were performed for each set of parameters.

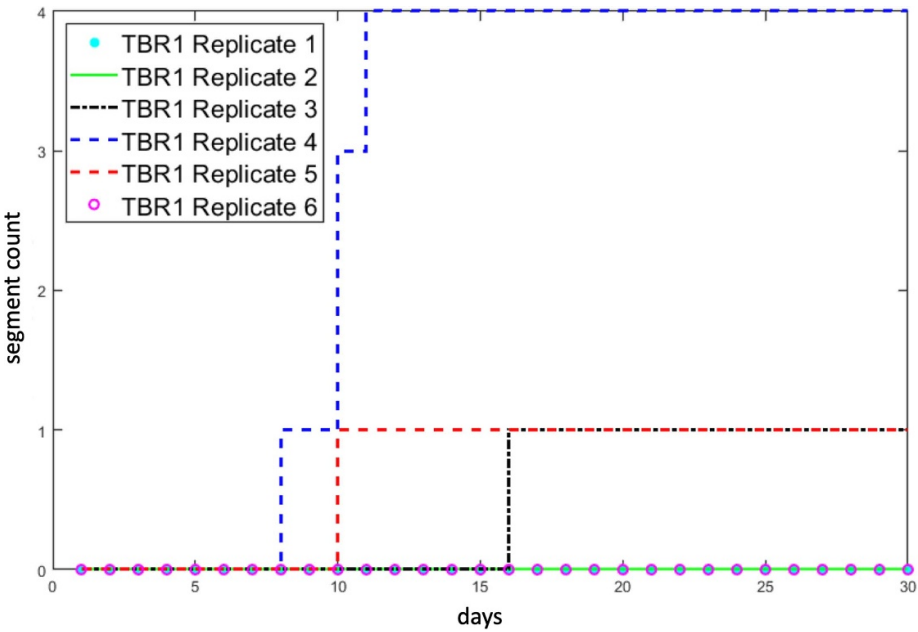


Figure C7. Number of *tbr1* segment counts appearing in TBR1 mat expansion experiments.

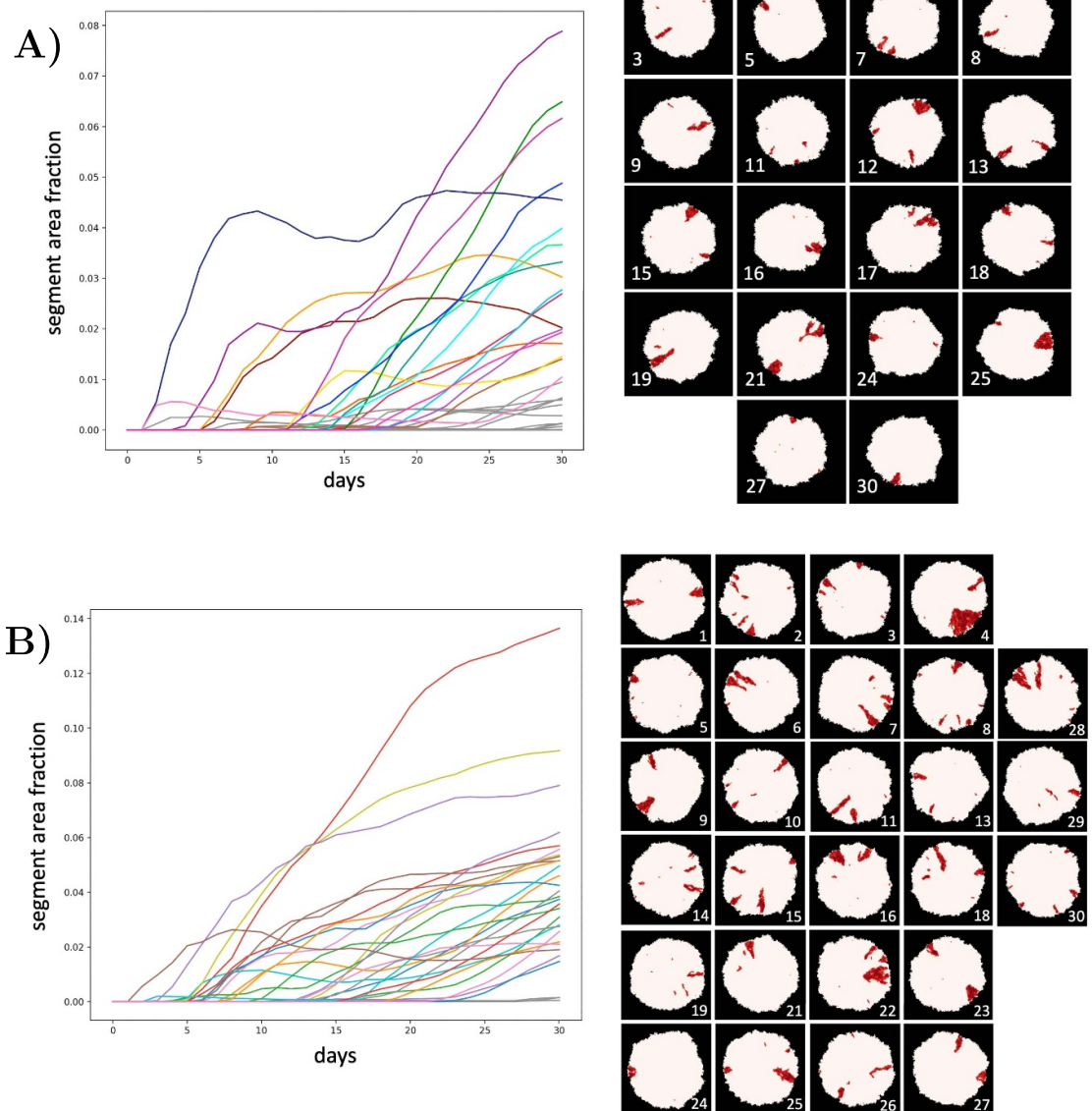


Figure C8. *In-silico* growth of rough-surface, pattern-forming TBR1 seeded mats. Plots for the area fraction of the smooth-surface phenotype over the course of 30 d of simulated growth with mutation to smooth-surface (*MT*) cells in a resident rough-surface (*WT*) mat. The segment area fraction is given by dividing the number of demes with a frequency of smooth-surface cells greater than 0.5 by the total number of occupied demes. Those that had a final area fraction above the threshold 0.01 were considered 'visible' and are plotted in colour. Images of these mats at the end of the simulation are shown on the right. Demes were coloured according to the frequency of the smooth-surface cells present, using a gradient from white for smooth-surface cells to dark red for rough-surface cells. 30 simulation replicates were performed for each set of parameters. Parameters were as follows: (A) $K_{WT} = 30$ cells/deme, $K_{MT} = 90$ cells/deme, $m_{WT} = 0.075$, $m_{MT} = 0.05$, and $r = 0.24 \text{ h}^{-1}$. (B) $K_{WT} = 30$ cells/deme, $K_{MT} = 90$ cells/deme, $m_{WT} = 0.10$, $m_{MT} = 0.075$, and $r = 0.24 \text{ h}^{-1}$.

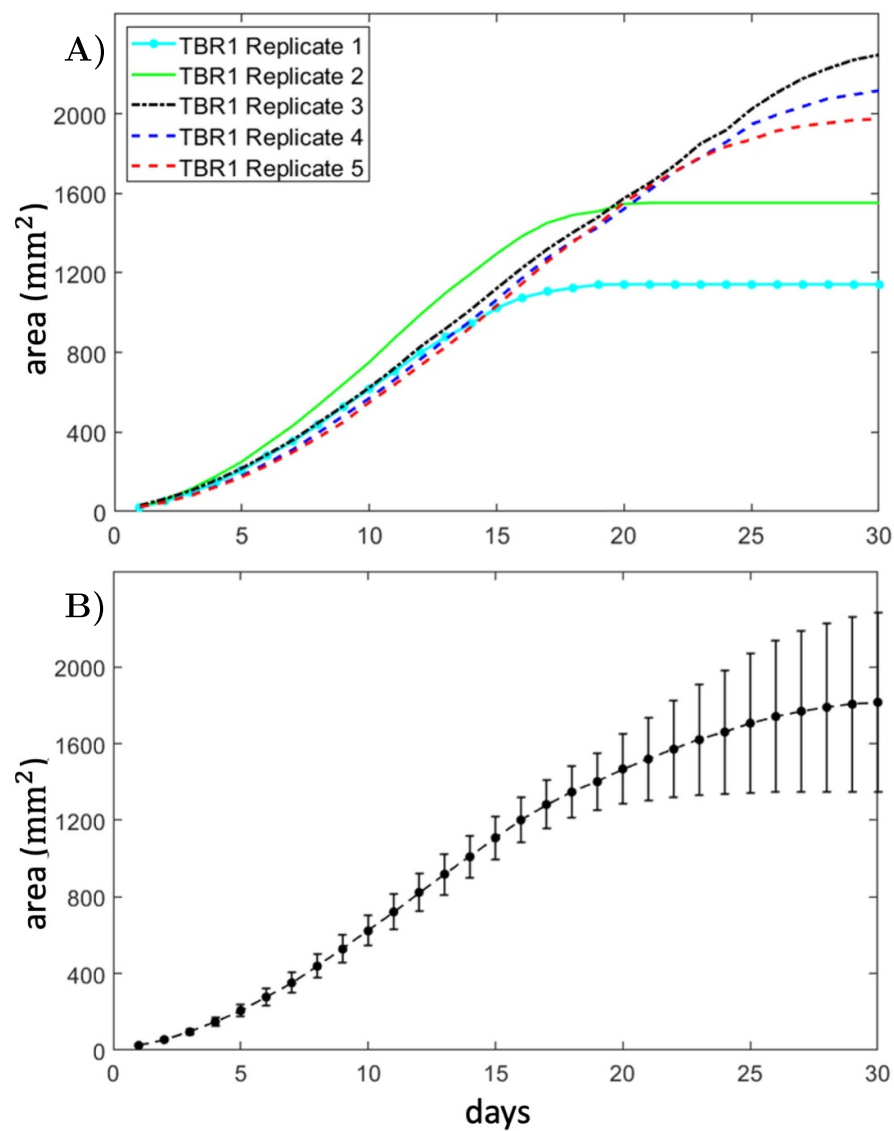


Figure C9. Area expansion of TBR1 mats. (A) Area expansion of individual mats over 30 d. (B) Average and standard deviation of the area expansion for five replicates. Data of TBR1 replicate 6 is not included due to contamination, which interfered with expansion of the mat.

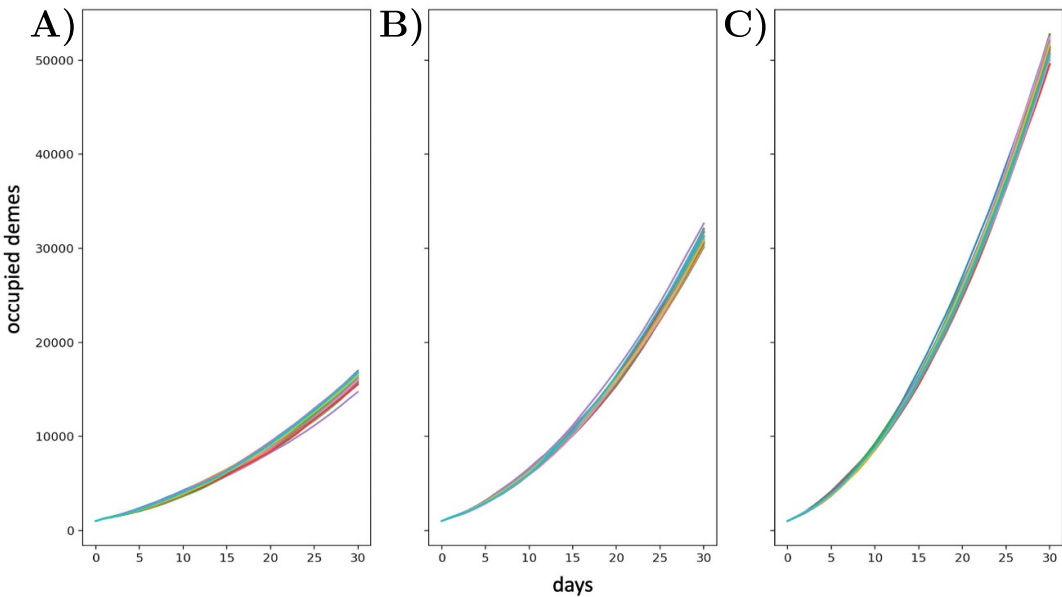


Figure C10. Area expansion of simulated mats over 30 days given by the number of occupied demes. Mats were seeded with rough-surface (*WT*) cells and allowed to mutate to a smooth-surface phenotype (*MT*). For all cases shown, the rough-surface carrying capacity was set to $K_{WT} = 30$ cells/deme and the smooth-surface carrying capacity was $K_{MT} = 90$ cells/deme. Expansion rate parameters increase from left to right as follows: (A) $m_{WT} = 0.05$ and $m_{MT} = 0.025$, (B) $m_{WT} = 0.075$ and $m_{MT} = 0.05$, (C) $m_{WT} = 0.10$ and $m_{MT} = 0.075$. For each set of parameters, 30 replicates were performed. The initial frequency of rough-surface cells was 0 and all cells had an intrinsic growth rate of $r = 0.24 \text{ h}^{-1}$.

Appendix D. Supplementary tables

Table D1. Parameter values and mean final frequencies (\bar{p}_{MT}) for simulations of head-to-head competition between rough-surface (*WT*) and smooth-surface (*MT*) mat phenotypes. A range of different carrying capacities (K (cells/deme)) and expansion rates (m) were considered and for each set of parameters. 30 replicates simulating 50 days of growth were performed. The initial frequency of smooth-surface cells was 0.5 and all cells had an intrinsic growth rate of $r = 0.24 \text{ h}^{-1}$, as measured in liquid media growth experiments. To simulate neutral competition, mutations were not considered.

K_{WT}	m_{WT}	K_{MT}	m_{MT}	final \bar{p}_{MT}
30	0.05	60	0.025	0.0741
30	0.05	90	0.025	0.3422
30	0.075	60	0.025	0.0205
30	0.075	60	0.05	0.0601
30	0.075	90	0.025	0.0337
30	0.075	90	0.05	0.3928
30	0.1	60	0.025	0.0098
30	0.1	60	0.05	0.0160
30	0.1	60	0.075	0.0461
30	0.1	90	0.025	0.0137
30	0.1	90	0.05	0.0364
30	0.1	90	0.075	0.3518
60	0.05	90	0.025	0.0467
60	0.075	90	0.025	0.0147
60	0.075	90	0.05	0.0369
60	0.1	90	0.025	0.0074
60	0.1	90	0.05	0.0115
60	0.1	90	0.075	0.0311

Table D2. Parameter values, mean final frequencies (\bar{p}_{MT}), and mean final segment area fractions ($\bar{A}_{\text{segment frac}}$) for simulations of mutations to the smooth-surface strain (*MT*) in a resident rough-surface (*WT*) population. A range of different carrying capacities (K (cells/deme)) and expansion rates (m) were considered for each parameter set. 30 replicates simulating 30 d of growth were performed. The initial frequency was of smooth-surface cells was 0 and all cells had an intrinsic growth rate of $r = 0.24 \text{ h}^{-1}$, as measured in liquid media growth experiments. The segment area fraction was calculated by dividing the number of demes with a frequency of smooth-surface cells greater than 0.5 by the total number of occupied demes.

K_{WT}	m_{WT}	K_{MT}	m_{MT}	\bar{p}_{MT}	$\bar{A}_{\text{segment frac}}$
30	0.05	60	0.025	0.0015	0.0026
30	0.05	90	0.025	0.0133	0.0171
30	0.075	60	0.025	0.0008	0.0014
30	0.075	60	0.05	0.0038	0.0062
30	0.075	90	0.025	0.0021	0.0030
30	0.075	90	0.05	0.0170	0.0217
30	0.1	60	0.025	0.0006	0.0010
30	0.1	60	0.05	0.0009	0.0016
30	0.1	60	0.075	0.0045	0.0075
30	0.1	90	0.025	0.0013	0.0019
30	0.1	90	0.05	0.0042	0.0059
30	0.1	90	0.075	0.0320	0.0408
60	0.05	90	0.025	0.0012	0.0003
60	0.075	90	0.025	0.0009	4.197×10^{-5}
60	0.075	90	0.05	0.0022	0.0004
60	0.1	90	0.025	0.0007	1.304×10^{-5}
60	0.1	90	0.05	0.0009	2.221×10^{-5}
60	0.1	90	0.075	0.0027	0.0005



Table D3. Parameter values, mean final frequencies (\bar{p}_{MT}), and mean final segment area fractions ($\bar{A}_{\text{segment frac}}$) for simulations of mutations to the rough-surface strain (*MT*) in a resident smooth-surface (*WT*) population. A range of different carrying capacities (K (cells/deme)) and expansion rates (m) were considered and for each parameters set. 30 replicates simulating 30 days of growth were performed. The initial frequency was of smooth-surface cells was 1 and all cells had an intrinsic growth rate of $r = 0.24 \text{ h}^{-1}$, as measured in liquid media growth experiments. The segment area fraction was calculated by dividing the number of demes with a frequency of smooth-surface cells less than 0.5 by the total number of occupied demes.

K_{WT}	m_{WT}	K_{MT}	m_{MT}	\bar{p}_{MT}	$\bar{A}_{\text{segment frac}}$
30	0.05	60	0.025	5.300×10^{-6}	0.0
30	0.05	90	0.025	0.0004	0.0002
30	0.075	60	0.025	5.530×10^{-6}	0.0
30	0.075	60	0.05	0.0076	0.0067
30	0.075	90	0.025	4.732×10^{-6}	0.0
30	0.075	90	0.05	6.448×10^{-6}	0.0
30	0.1	60	0.025	9.947×10^{-6}	0.0
30	0.1	60	0.05	0.0084	0.0077
30	0.1	60	0.075	0.0016	0.0012
30	0.1	90	0.025	1.106×10^{-5}	0.0
30	0.1	90	0.05	0.0002	0.0001
30	0.1	90	0.075	0.0006	0.0003
60	0.05	90	0.025	2.550×10^{-5}	0.0
60	0.075	90	0.025	1.649×10^{-5}	0.0
60	0.075	90	0.05	0.0054	0.0055
60	0.1	90	0.025	0.0009	0.0055
60	0.1	90	0.05	5.035×10^{-5}	4.196×10^{-6}
60	0.1	90	0.075	2.026×10^{-5}	0.0

Table D4. Parameter values, mean final frequencies (\bar{p}_{MT}), and mean final segment area fractions ($\bar{A}_{\text{segment frac}}$) for simulations of neutral mutations. A range of different carrying capacities (K (cells/deme)) and expansion rates (m) were considered and for each parameter set, 30 replicates simulating 30 days of growth were performed. The initial frequency of mutated cells was 0 and all cells had an intrinsic growth rate of $r = 0.24 \text{ h}^{-1}$, as observed in liquid media growth experiments. Mutations were neutral (i.e. mutant cells had the same carrying capacity and expansion rate as resident cells). The segment area fractions was calculated by dividing the number of demes with a frequency of smooth-surface cells greater than 0.5 by the total number of occupied demes.

K	m	\bar{p}_{MT}	$\bar{A}_{\text{segment frac}}$
30	0.025	8.906×10^{-6}	0.0
30	0.05	3.225×10^{-5}	8.505×10^{-6}
30	0.075	2.265×10^{-5}	1.033×10^{-6}
30	0.1	3.246×10^{-5}	7.219×10^{-6}
60	0.025	2.938×10^{-5}	5.364×10^{-6}
60	0.05	2.872×10^{-5}	0.0
60	0.075	1.454×10^{-4}	1.038×10^{-4}
60	0.1	7.396×10^{-5}	1.976×10^{-5}
90	0.025	4.413×10^{-5}	0.0
90	0.05	6.009×10^{-5}	1.410×10^{-5}
90	0.075	5.728×10^{-5}	1.067×10^{-6}
90	0.1	9.175×10^{-5}	4.587×10^{-6}

ORCID iDs

Rebekah Hall  <https://orcid.org/0000-0003-0113-429X>
Daniel A Charlebois  <https://orcid.org/0000-0001-7426-1789>

References

[1] Rainey P B and Travisano M 1977 Adaptive radiation in a heterogeneous environment *Phil. Trans. R. Soc. B* **280** 29–101

[2] Kerr B, Neuhauser C, Bohannan B J M and Dean A M 2006 Local migration promotes competitive restraint in a host–pathogen ‘tragedy of the commons’ *Nature* **442** 75–78

[3] Coberly L C, Wei W, Sampson K Y, Millstein J, Wichman H A and Krone S M 2009 Space, time and host evolution facilitate coexistence of competing bacteriophages: theory and experiment *Am. Nat.* **173** E121–38

[4] Klopstein S, Currat M and Excoffier L 2006 The fate of mutations surfing on the wave of a range expansion *Mol. Biol. Evol.* **23** 482–90

[5] Travis J M J, Münkemüller T, Burton O J, Best A, Dytham C and Johst K 2007 Deleterious mutations can surf to high densities on the wave front of an expanding population *Mol. Biol. Evol.* **24** 2334–43

[6] Hallatschek O, Hersen P, Ramanthan S and Nelson D R 2007 Genetic drift at expanding frontiers promotes gene segregation *Proc. Natl Acad. Sci. USA* **104** 19926–30

[7] Hallatschek O and Nelson D R 2008 Gene surfing in expanding populations *Theor. Popul. Biol.* **73** 158–70

[8] Peischl S, Dupanloup I, Kirkpatrick M and Excoffier L 2013 On the accumulation of deleterious mutations during range expansions *Mol. Ecol.* **22** 5972–82

[9] Hallatschek O and Nelson D R 2009 Life at the front of an expanding population *Evolution* **64** 193–206

[10] Gralka M, Stiewe F, Farrell F, Möbius W, Waclaw B and Hallatschek O 2016 Allele surfing promotes microbial adaptation from standing variation *Ecol. Lett.* **19** 889–98

[11] Miller T E X et al 2020 Eco-evolutionary dynamics of range expansion *Ecology* **101** e03139

[12] Roughgarden J 1971 Density-dependent natural selection *Ecology* **52** 453–68

[13] Deforet M, Carmona-Fontaine C, Korolev K S and Xavier J B 2019 Evolution at the edge of expanding populations *Am. Nat.* **194** 291–305

[14] Shine R, Brown G P and Phillips B L 2011 An evolutionary process that assembles phenotypes through space rather than through time *Proc. Natl Acad. Sci. USA* **108** 5708–11

[15] Travis J M J and Dytham C 2002 Dispersal evolution during invasions *Evol. Ecol.* **4** 1119–29

[16] Simmons A D and Thomas C D 2004 Changes in dispersal during species’ range expansions *Am. Nat.* **164** 378–95

[17] Phillips B L and Perkins T A 2019 Spatial sorting as the spatial analogue of natural selection *Theor. Ecol.* **12** 155–63

[18] Burton O J, Phillips B L and Travis J M J 2010 Trade-offs and the evolution of life-histories during range expansion *Ecol. Lett.* **13** 1210–20

[19] Ochocki B M, Saltz J B and Miller T E X 2020 Demography-dispersal trait correlations modify the eco-evolutionary dynamics of range expansion *Am. Nat.* **195** 231–46

[20] Wortel M T, Noor E, Ferris M, Bruggeman F J and Liebermeister W 2018 Metabolic enzyme cost explains variable trade-offs between microbial growth rate and yield *PLoS. Comput. Biol.* **14** e1006010

[21] Urquhart-Cronish M, Angert A L, Otto S P and MacPherson A 2024 Density-dependent selection during range expansion affects expansion load in life-history traits *Am. Nat.* accepted (<https://doi.org/10.1086/728599>)

[22] Lo W-S and Dranginis A M 1998 The cell surface flocculin flo11 is required for pseudohyphae formation and invasion by *Saccharomyces cerevisiae* *Mol. Biol. Cell* **9** 161–71

[23] Guo B, Styles C A, Feng Q and Fink G R 2000 A *Saccharomyces* gene family involved in invasive growth, cell-cell adhesion and mating *Proc. Natl Acad. Sci. USA* **97** 12158–63

[24] Reynolds T B, Jansen A, Peng X and Fink G R 2008 Mat formation in *Saccharomyces cerevisiae* requires nutrient and pH gradients *Eukaryotic Cell* **7** 122–30

[25] Reynolds T B 2018 Going with the flo: the role of flo11-dependent and independent interactions in yeast mat formation *J. Fungi* **4** 132

[26] Chen L, Noorbakhsh J, Adams R M, Samaniego-Evans J, Agollah G, Nevozhay D, Kuzdzal-Fick J, Mehta P and Balázs G 2014 Two-dimensionality of yeast colony expansion accompanied by pattern formation *PLoS Comput. Biol.* **10** e1003979

[27] Reynolds T B and Fink G R 2001 Bakers’ yeast, a model for fungal biofilm formation *Science* **291** 878–81

[28] Váchová L, Šťovíček V, Hlaváček O, Chernyavskiy O, Štěpánek L, Kubínová L and Palková Z 2011 Flo11p, drug

22

- efflux pumps and the extracellular matrix cooperate to form biofilm yeast colonies *J. Cell Biol.* **194** 679–87
- [29] Gillespie D T 1977 Exact stochastic simulation of coupled chemical reactions *J. Phys. Chem.* **81** 2340–61
- [30] Korolev K S, Avlund M, Hallatschek O and Nelson D R 2010 Genetic demixing and evolution in linear stepping stone models *Rev. Mod. Phys.* **82** 1691–718
- [31] Korolev K S, Xavier J B, Nelson D R and Foster K R 2011 A quantitative test of population genetics using spatio-genetic patterns in bacterial colonies *Am. Nat.* **178** 538–52
- [32] Kimura M and Weiss G H 1964 The stepping stone model of population structure and the decrease of genetic correlation with distance *Genetics* **49** 561–76
- [33] Charlebois D A and Balázsi G 2019 Modeling cell population dynamics *In Silico Biol.* **13** 21–39
- [34] Verstrepen K J, Reynolds T B and Fink G R 2004 Origins of variation in the fungal cell surface *Nat. Rev. Microbiol.* **2** 533–40
- [35] Gemayel R, Vignes M D, Legendre M and Verstrepen K J 2010 Variable tandem repeats accelerate evolution of coding and regulatory sequences *Annu. Rev. Genet.* **44** 445–77
- [36] Hall R 2023 (available at: <https://github.com/bekahall/meta-colony-model>)
- [37] Rasband W S ImageJ. U.S National Institute of Health, Bethesda, Maryland, USA 1997–2018 (available at: <https://imagej.net/ij/index.html>)
- [38] Bandara A 2023 (available at: <https://data.mendeley.com/datasets/xb4r9vbh7x/1>)
- [39] Verstrepen K J, Jansen A, Lewitter F and Fink G R 2005 Intragenic tandem repeats generate functional variability *Nat. Genet.* **37** 986–90
- [40] Foutel-Rodier F and Etheridge A M 2020 The spatial Muller's ratchet: surfing of deleterious mutations during range expansion *Theor. Popul. Biol.* **135** 19–31
- [41] Carson H L 1987 The genetic system, the deme and the origin of species *Annu. Rev. Genet.* **21** 405–23
- [42] Peischl S and Excoffier L 2015 Expansion load: recessive mutations and the role of standing genetic variation *Mol. Ecol.* **24** 2084–94
- [43] Nadell C D, Foster K R and Xavier J B 2010 Emergence of spatial structure in cell groups and the evolution of cooperation *PLoS Comput. Biol.* **6** e1000716
- [44] Salama O E and Gerstein A C 2021 High-throughput computational analysis of biofilm formation from time-lapse microscopy *Curr. Protocols* **1** e194
- [45] Hall R and Charlebois D A 2021 Lattice-based monte carlo simulation of the effects of nutrient concentration and magnetic field exposure on yeast colony growth and morphology *In Silico Biol.* **14** 53–69
- [46] Charlebois D A and Balázsi G 2016 Frequency-dependent selection: a diversifying force in microbial populations *Mol. Syst. Biol.* **12** 880
- [47] Healey D, Axelrod K and Gore J 2016 Negative frequency-dependent interactions can underlie phenotypic heterogeneity in a clonal microbial population *Mol. Syst. Biol.* **12** 877
- [48] Gou L, Bloom J S and Kruglyak L 2019 The genetic basis of mutation rate variation in yeast *Genetics* **211** 731–40
- [49] Lo W S and Dranginis A M 1996 Flo11, a yeast gene related to the STA genes, encodes a novel cell surface flocculin *J. Bacteriol.* **178** 7144–51
- [50] Yanoff M and Duker J S 2009 *Ophthalmology* 3rd edn (Elsevier) p 54